International Journal of Heat and Mass Transfer 222 (2024) 125109

Contents lists available at ScienceDirect

International Journal of Heat and Mass Transfer

journal homepage: www.elsevier.com/locate/ijhmt

Modeling of growth and dynamics of droplets during dropwise condensation of steam

Matteo Mirafiori, Marco Tancon, Stefano Bortolin *, Davide Del Col

Dipartimento di Ingegneria Industriale, Università degli Studi di Padova, Via Venezia 1, Padova 35131, Italy

ARTICLE INFO

Keywords:
Dropwise condensation
Droplet population
Droplet dynamics
Condensation heat transfer
Numerical simulation

ABSTRACT

Computational modeling is essential for understanding dropwise condensation (DWC) mechanisms, droplet life-cycle, and predicting heat transfer. However, the multiscale nature of DWC increases the computational cost, thus making the study of the droplet distribution more difficult. Population-based models available in the literature rely on empirical or statistical methods for determining the drop-size distribution. Differently, in the present study, a new individual-based model developed in hybrid MATLAB® and C codes and based on parallel computing is developed to simulate the whole dropwise condensation process, addressing the growth of each droplet, without making any assumption on the droplet population and considering a number of drops never reached in previous similar studies. The proposed model's computational efficiency is significantly improved when considering more than 1 million drops in the computational domain. To optimize the calculation time, the effects of time step, computational domain size, and simulation duration on the overall heat flux and drop-size distribution are discussed. The numerical results are compared against predictions from population-based models available in the literature. The proposed model is also used to study the droplet population and the instantaneous heat flux during DWC at different positions along a vertical condensing surface (upper, middle and lower areas). As a final step, a preliminary comparison is carried out between the present model and experimental data acquired during dropwise condensation on a nearly hydrophobic vertical surface. Considering a nucleation size density of 5×10^{12} m^{-2} (11×10^{6} drops in the computational domain), the simulation is able to predict the experimental heat flux and the large drop-size distribution.

1. Introduction

The condensation phase-change process is ubiquitous in nature and it is exploited in many engineering applications such as thermal power plants [1], chemical refining [2], seawater desalinization [3], refrigeration [4], and electronics cooling [5,6]. Improving the effectiveness of the condensation heat transfer process can lead to a reduction of the energy consumption of the system inside which condensation takes place: dropwise condensation is a passive solution that can enhance the condensation heat transfer process with economic benefits and minor CO_2 emissions [7].

Commonly, a vapor on a cooled surface can condense in two ways, either by the formation of a continuous liquid film (filmwise condensation) or by the formation of discrete droplets (dropwise condensation). The surface wettability plays a key role in the selection of the type of condensation mode. The wettability can be described by measuring the static contact angle θ or the dynamic contact angles. The advancing contact angle (θ_{adv}) is defined when the droplet moves forward toward a non-wetted surface, while the receding angle (θ_{rec}) when the droplet moves across a wet surface [8]. Due to the removal of the continuous liquid film, the heat transfer coefficient (HTC) during dropwise condensation (DWC) of pure water vapor can be 5–7 times higher compared to filmwise condensation (FWC) [9–11].

During DWC, the small droplets that nucleate at preferential sites grow by direct condensation and coalescence until they reach the critical dimension at which they start to move, sweeping the surface and making new nucleation sites available. In a recent paper, Maggiolo et al. [12] have shown that promoting DWC in a plate heat exchanger can improve both HTC and self-cleaning from fouling. The peculiar feature of DWC is that many processes coexist at different temporal and spatial scales, with the time scale ranging from microsecond to second and the spatial scale ranging from nanometer to few millimeters. Furthermore, the processes such as growth, coalescence and sliding can occur simultaneously [13,14]. Several researchers [7,15–17] have studied the droplet dynamics using advanced optical techniques, carrying out studies down to the

* Corresponding author.
E-mail address: stefano.bortolin@unipd.it (S. Bortolin).

https://doi.org/10.1016/j.ijheatmasstransfer.2023.125109
Received 26 January 2023; Received in revised form 7 April 2023; Accepted 18 December 2023

Nomenclature

A	area, m^2
a	droplet acceleration, m s^{-2}
Bi	Biot number, -
C_d	drag coefficient, -
c_p	specific heat capacity, J kg^{-1} K^{-1}
d	distance, m
G	growth rate dr/dt, m s^{-1}
F	force, N
g	gravitational acceleration, m s^{-2}
h_i	interfacial heat transfer coefficient, W m^{-2} K^{-1}
h_{lv}	latent heat of vaporization, J kg^{-1}
HTC	heat transfer coefficient, kW m^{-2} K^{-1}
k	coverage factor, -
k_c	retention factor, -
l	length/height, m
L_{ch}	channel height, m
$\dot{m}$	mass flow rate, kg s^{-1}
$\overline{M}_v$	molecular mass, kg $kmol^{-1}$
n	droplet number, -
$n(r)$	small droplet population density function, m^{-3}
$N(r)$	large droplet population density function, m^{-3}
N_s	nucleation site density, m^{-2}
Nu	Nusselt number, -
Q	heat flow rate, W
q	heat flux, kW m^{-2}
$\tilde{q}$	instantaneous heat flux, kW m^{-2}
r	radius, m
$\overline{R}$	universal gas-constant, 8314.46 J $kmol^{-1}$ K^{-1}
Re	Reynolds number, -
T	temperature, K
t	time, s
v	velocity, m s^{-1}
z	orthogonal axis of the sample, m
z_1	position (1.3 mm) along z, m
z_2	position (2.8 mm) along z, m

Greek symbols

α	accommodation factor, -
δ	thickness, nm
ε	efficiency, -
ΔT	temperature difference, K
Δt	time difference, s
$\Delta\theta$	contact angle hysteresis, °
$\Delta\tau$	simulation time step, s
θ	contact angle, °
λ	thermal conductivity, W m^{-1} K^{-1}
ρ	density, kg m^{-3}
σ	surface tension, N m^{-1}

Subscripts

0	initial
adv	advancing
ad	adhesion
AL	aluminum
b	base
cool	coolant side
d	droplet
dr	drag
DWC	dropwise
e	effective
g	gravity
HC	hydrophobic coating
in	test section inlet
l	liquid
max	maximum
min	minimum
out	test section outlet
real	real
rec	receding
sat	saturation
sim	simulation
v	vapor
wall	wall

micrometric scale. However, it is impossible to experimentally observe and collect data on the dynamics of droplets in saturated pure steam conditions and with droplets dimensions from micrometers down to nanometers. Therefore, researchers are forced to investigate DWC through theoretical and computational studies. It should be noted that, due to the multiscale nature of DWC, the study from a computational point of view is very challenging.

In order to calculate the overall heat flux transferred during DWC, the most used approach in the literature [18–21] is to combine the heat transfer through a single drop (analytically or numerically determined) with the drop-size distribution (statistically or empirically calculated). To estimate the heat transfer through a single droplet, a network of thermal resistances from the saturated vapor to the subcooled surface is usually employed [21–24]. Instead, the drop-size density is usually evaluated by considering a semi-empirical law for larger droplets (which grow mainly by coalescence) and statistical considerations for small drops (which grow by direct condensation). The drop-size distribution of the small drops in steady-state conditions can be analytically obtained by solving the population balance theory [25,26]. Hereinafter, this kind of approach is referred to as the population-based model (PBM). Another method to calculate the drop-size distribution (of both small and large drops) is to use a numerical simulation, in which the growth of the individual drops is followed throughout their life cycle without any statistical assumption. Models based on this approach are defined as the individual-based models (IBMs). It should be noted that both the PBM and IBM requires a model for the heat transfers through a single drop. Due to the aforementioned limitations related to the capability of the present optical systems in detecting nucleation sites, neither the drop-size distribution evaluated by the PBM nor that given by the IBM can be experimentally validated.

The first formulation of the heat transfer through a single droplet was proposed by Rose [18,19] and it accounts for the thermal resistance due to conduction through the droplet, the vapor-liquid interfacial resistance, the conduction resistance through the coating, and the temperature drop due to droplet curvature. Kim and Kim [21] developed a model valid for hydrophobic surfaces. In their work, the heat transfer through a single drop is estimated by considering the thermal resistance network from the vapor to the subcooled surface as proposed by Rose [19], but they analytically solve the conduction resistance through the drop. Furthermore, the authors [21] improved the formulation of the thermal resistances of the coating layer. Miljkovic et al. [22] extended the Kim and Kim [21] model to nanostructured superhydrophobic surfaces by taking into account the surface morphology. In the case of a flat surface (with no microstructure), the two models [21,22] lead to the same results in terms of heat transfer through a single drop. With the aim of improving the modelling of the conduction resistance through the drop, Chavan et al. [23] performed numerical simulations by varying the Biot number and the contact angle θ to determine the conduction resistance for drops with contact angles greater than 90° and Biot numbers larger than 0.1. More recently, Lethuillier et al. [24], based on the work of

Chavan et al. [23], improved the function for the determination of the conduction resistance by expanding both the interval of Biot number (from 10^{-4} to 10^{5}) and contact angle (from 20° to 170°). Since data on single droplet growth is lacking and the drop-size distribution is not known a priori, no single droplet heat transfer model has ever been directly or indirectly validated against DWC experimental data.

In 1966, Le Fevre and Rose [27], starting from the experimental data obtained by different authors [28,29], proposed a semi-empirical model to predict the density function for large droplets population. Their model has recently been validated by several authors [7,15,30] against experimental data. However, since the model is based on data collected on the large droplet population, whose growth is mainly due to coalescence, it is not suitable to properly describe the drop-size distribution of small droplets, whose growth is dominated by direct vapor condensation. Wu and Maa [31] obtained the first formulation of the drop-size distribution of small drops by assuming that heat conduction through the droplets is the only thermal resistance in the droplet growth process. Later, Maa [32] derived a first formulation of the population balance theory by considering that the number of drops that enter a given radii range is equal to the number of drops that grow and leave the radii class by direct condensation. In the resulting equation, the number of nucleation sites was varied to fit the experimental data [33,34]. Tanaka [25,26], analyzing the videos of a surface vertically oriented, inferred that during steady-state dropwise condensation the condensing surface is periodically swept by the sliding drops. Therefore, based on statistical and geometric considerations, the author modified the population balance theory by considering that the number of drops that enter a certain radii bin is equal to the number of drops that leave it both by direct condensation and by sweeping of sliding drops. It should be noted that the population balance theory (PBM) proposed by Tanaka [25,26] is still used nowadays. Differently from the previous works [25,31,32] in which only the droplet thermal conduction resistance is considered, Abu-Orabi [20] developed a PBM by considering all the thermal resistances involved in the condensation process: the liquid-vapor interfacial resistance, the temperature drop due to droplet curvature, the conduction resistances through the droplet and the promoter layer. Subsequently, Kim and Kim [21], combining their formulation of the thermal resistances with the population balance theory, obtained an analytical expression for the distribution of small drops. In their work, they introduced the effective radius r_e which is defined as the threshold radius between the distribution of small droplets and the distribution of large droplets. This parameter depends on how the nucleation sites are distributed on the surface; in their model, the nucleation sites are assumed to be regularly arranged. Miljkovic et al. [22] developed their PBM in which, unlike Kim and Kim [21], they considered a micro-structured promoter layer and a random distribution of the nucleation sites. As mentioned above, in the case of flat surfaces, the expression of the single droplet heat transfer is the same for the two models. However, the hypothesis of nucleation sites distribution is different: regularly arranged for Kim and Kim [21], while randomly distributed for Miljkovic et al. [22]. Therefore, the value of effective radius (r_e) is different in the two models, resulting in a slight variation of the drop-size distributions.

As an alternative to the PBM, many researchers have used numerical simulations (IBM) to study both the drop-size distribution and the dynamic processes (such as coalescence and sliding) that occur during DWC. However, the high nucleation sites density necessary to simulate DWC of steam ($N_s = 10^9 - 10^{15}$ m^{-2}) increases the computational cost of IBMs. To reduce the computational time, various simplifications have been introduced into the simulations, such as dividing the simulation into different stages [35], decreasing the number of nucleation sites [35–37], reducing the droplet maximum radius r_{max} to reduce the dimensions of the computational domain [37–39]. The idea of dividing the simulation into different stages proposed by Glicksman and Hunt [35] consists of simulating a variable computational domain according to the droplet size. In every next stage of the simulation, the surface area is increased by ten times and the large droplets formed from the previous stage are redistributed on the enlarged surface until droplets left the surface. However, despite the advantage from the computational point of view, droplet re-nucleation was not considered. Burnside et al. [40] simulated the primary stage of the condensation process (0.21 ms) considering a computational domain of 240 × 240 μm^2, a nucleation sites density $N_s = 10^{12}$ m^{-2} (with a number of drops equal to 57,600), and a time step of 0.23 μs, while the maximum radius was fixed at 4 μm. The authors focused on the droplet growth by coalescence, comparing the results with the theoretical model proposed by Le Fevre and Rose [27]. Meng et al. [41] simulated a domain of 400 × 400 μm^2 and $N_s = 10^{10}$ m^{-2} (with a number of drops equal to 1600), a time step of 10 ms, and a departing radius of 15 μm. With their IBM, the authors compared the heat flux obtained numerically with the experimental data acquired by Wen et al. [42] on a superhydrophobic surface. However, no information on the drop-size distribution was provided. To study the effect of surface wettability on the distribution of large droplets, Xu et al. [37] performed numerical simulations considering an area of 4 × 4 mm^2, a time step of 1 μs, a nucleation sites density of 10^{10} m^{-2} (the drops number over the surface is 160,000), and a departing radius of 1 mm. Similarly, Mei et al. [43] focused on the instantaneous and time-averaged characteristics of the drop-size distribution, performing simulations at varying the nucleation sites density from 6.25 × 10^{11} to 10^{13} m^{-2} over a domain of 200 × 200 μm^2 (r_{max} = 16 μm). Under these conditions, the number of simulated drops ranged from 25,000 to 400,000. Hu et al. [44] improved the IBM of Meng et al. [41] by developing an event-driven IBM able to numerically simulate superhydrophobic surface but without giving any information on the droplet distribution. In their work, they considered a nucleation site density of 4 × 10^{10} m^{-2} over a computational domain of 1 × 1 mm^2 (thus the maximum number of simulated drops was equal to 40,000). The time step was variable in the range 1–10 ms, while the departing radius was chosen according to the departing mechanism: r_{max} = 15 μm for jumping drops, r_{max} = 100 μm for sliding drops.

From the literature survey it emerges that, due to the large droplet departing radii, the dynamic process of DWC on hydrophilic and hydrophobic surfaces has been marginally addressed with numerical simulations. In fact, the larger the departing radius (as in the case of hydrophilic surfaces), the wider the computational domain of the simulation and the higher the number of drops for the same nucleation site density. Therefore, until now, the researchers have focused on DWC simulations on superhydrophobic surfaces (with small droplet departing radius). Instead, the IBMs have not been used to study dropwise condensation on hydrophobic surfaces or hydrophilic surfaces with a low hysteresis of the contact angle ($\Delta\theta = \theta_{adv} - \theta_{rec}$), thus excluding most of the promising heat transfer surfaces [7,30,45]. Computational investigations are needed to improve the knowledge of DWC phenomenon but, since the numerical simulations of DWC of pure vapor have enormous computational costs, it is crucial to optimize the algorithms to obtain reliable results in terms of both heat flux and droplet populations.

Considering the gaps described above, in the present work a new DWC numerical model based on the simulation of growth of each droplet without making statistical assumptions on the droplet population and considering a number of drops never reached in previous IBM studies is presented. The strength of the model is the multicore parallel computing obtained by developing a hybrid C programming language & MATLAB® algorithm in which the C code is used to solve the iterative calculations and the MATLAB® code is used to achieve efficient storage and retrieval of data. The main parameters of the numerical model (such as the time step, the size of the computational domain, and the simulation time) were optimized to find the best compromise between computational cost and accuracy in the simulation results. The present individual-based model (IBM) is applied to investigate the effect of the number of nucleation sites on the calculated heat flux and droplet distribution and compared to a population-based model (PBM). Furthermore, the present model is used to study the effect of sliding droplets on a vertically

oriented computational domain with a large height-to-width aspect ratio, by evaluating the drop-size distribution and the heat flux in three different portions of the surface (upper, central, and lower areas). Finally, the experimental data obtained using the experimental apparatus presented by Tancon et al. [30] are compared with those numerically obtained by simulating a maximum of 11,250,000 drops ($N_s = 5 \times 10^{12}$ m^{-2}) on a nearly hydrophobic surface ($\theta_e = 77°$, $r_{max} = 0.7$ mm), finding a good agreement in terms of heat flux and drop-size distributions.

2. Numerical method

In this Section, a detailed description of the present individual-based model (IBM) developed to simulate dropwise condensation is provided.

The individual-based model (IBM) assumes that the nucleation sites are randomly distributed over the condensing surface (calculation domain) following a Poisson distribution and the droplet growth/interaction processes are governed by physics-based equations. For fixed thermodynamic conditions and nucleation sites density, by evaluating the position and size of the drops over time within the domain, the model allows to calculate the drop-size distributions (of small and large droplets) and the instantaneous heat flux. The flowchart of the present IBM is depicted in Fig. 1.

Once the nucleation sites have been randomly positioned on the simulation domain, a droplet with a radius equal to radius of the smallest thermodynamically viable drop r_{min} (Eq. (1)) is placed on each nucleation site. Each drop is fully characterized by its curvature radius r and the coordinates of its center (x, y). During the simulation, the drops can grow, coalesce and slide, cleaning the underlying surface and exposing new nucleation sites. Therefore, the dropwise condensation process can be repeated quasi-cyclically [46]. The simulation ends when quasi-stationary conditions are reached.

The present IBM was developed using both MATLAB® and C programming languages. MATLAB® was chosen as the main environment to control the calls of the different functions and store the vectors, while C was used for a more efficient solution of the invoked subroutines. The functions for modelling droplets growth, coalescence, and sliding require considerable computational power and a large amount of memory, which gradually increase with the number of droplets in the simulation domain. In order to reduce the computational time, parallel computing was implemented by dividing the operations on all available CPU cores by means of the library OpenMP. The drop-size distribution and the instantaneous heat flux are obtained from the results of the simulation. The drop-size distribution is calculated by dividing the interval of droplet radii from r_{min} to the r_{max} into different bins and counting the number of droplets whose radius falls within each bin. Instead, the instantaneous heat flux depends on the model chosen for the heat transfer through a single droplet (see Section 2.2) and it is calculated as the sum of the heat transferred by each droplet on the surface. According to the literature for hydrophilic and hydrophobic surfaces [21,22,47], a constant droplet contact angle is assumed during the droplet life cycle. With regards to the sweeping mechanism, differently from other IBMs in the literature which assume a constant droplet sliding velocity [38,39], the present IBM considers a constant droplet acceleration according to the experimental work by Tancon et al. [48]. Furthermore, the simulations assume the condensation of pure vapor, thus in the absence of non-condensable gases. The following Sections will provide further details on the modeling approach of each physical process occurring during DWC, with the descriptions of the main equations used in the numerical model.

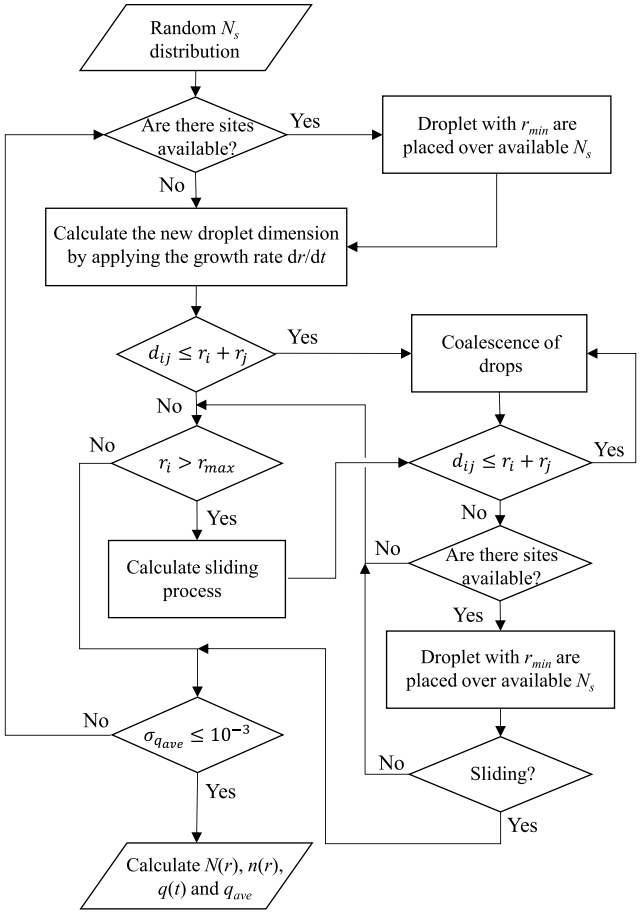

Fig. 1. Flowchart of the present IBM.

2.1. Nucleation

Before starting the numerical simulation, the nucleation sites are randomly distributed on the domain: both the nucleation site density (N_s) and the computational domain dimensions must be given as input to the model. The model assumes that the position of the nucleation sites does not change over time. Although the droplets do not physically nucleate at the same time [49], the simulation makes use of this hypothesis. Several studies in the literature [35,50] have shown that the drop-size distribution obtained from numerical simulations is not influenced either by the initial nucleation site distribution or by the instantaneous positioning of the droplets on the available nucleation sites. Furthermore, studying the first instants of water vapor condensation via Molecular Dynamics simulations, several researchers [51–53] have evaluated the time required for nucleation and this time results to be lower than the time step usually used in the numerical simulations. In particular, Ranathunga et al. [52] observed that, to form a drop with a radius equal to the minimum one, a time from 3 to 40 ns are required depending on the surface wettability (θ = 10–120°). Therefore, by appropriately choosing the time step to be used in the simulations, it is possible to assume that all the available nucleation sites in the next instant are occupied by a droplet. In the present simulations, a time step ($\Delta\tau$) of 10^{-5} s is usually considered (see Section 3.1 and 3.2 for further details); this value is in agreement with the hypothesis of instantaneous nucleation and, as will be discussed in Section 3.3 (Fig. 5), allows to adequately approximate the growth of the drops.

At each time step, a drop with a radius equal to r_{min} is placed in each free nucleation site. Unless otherwise stated, r_{min} is equivalent to the smallest thermodynamically viable drop, and it is obtained from:

$$r_{min} = \frac{2\,\sigma\,T_{sat}}{\rho_l\,h_{lv}\,\Delta T} \tag{1}$$

where σ is the surface tension, T_{sat} is saturation temperature, ρ_l is the liquid density, h_{lv} is the latent heat of vaporization and ΔT is the

temperature difference between the saturation and wall temperature.

2.2. Droplet growth

At each time step of the simulation, the droplets grow according to a specific model for the single drop heat transfer rate, Q_d. Among the models present in the literature, four studies have been selected in the present study: Kim and Kim [21], Miljkovic et al. [22], Chavan et al. [23] and Lethuillier et al. [24].

First, the model developed by Kim and Kim [21] and then updated by Miljkovic et al. [22] to take into account the surface morphology of superhydrophobic micro/nanostructured surfaces is considered. It should be noted that, in the case of a flat surface, the expression for the heat transfer though a single droplet by Miljkovic et al. [22] is equal to that by Kim and Kim [21], which can be expressed as:

$$Q_d = \frac{\pi r^2 \left(1 - \frac{r_{min}}{r}\right) \Delta T}{\frac{1}{2h_i(1-\cos\theta_e)} + \frac{r\theta_e}{4\lambda_l \sin\theta_e} + \frac{\delta_{HC}}{\lambda_{HC}\sin^2\theta_e}} \tag{2}$$

where r is the curvature radius, λ_l and λ_{HC} are respectively the thermal conductivity of the liquid droplet and the coating layer, δ_{HC} is the coating thickness, θ_e is the equilibrium contact angle $\theta_e = \cos^{-1}(0.5 \cos\theta_{adv} + 0.5 \cos\theta_{rec})$, and h_i is the heat transfer coefficient at the liquid-vapor interface, which can be calculated according to [54] as:

$$h_i = \left(\frac{2\alpha}{2-\alpha}\right) \frac{\rho_l h_{lv}^2}{T_{sat}} \left(\frac{\overline{M}_v}{2\pi \overline{R} T_{sat}}\right)^{1/2} \tag{3}$$

where $\overline{M}_v$ is the molecular mass of the vapor, $\overline{R}$ is the universal gas-constant, and α is accommodation condensation coefficient. The latter expresses the ratio of the amount of vapor mass flux that actually enters the liquid phase to the total vapor mass flux impinging on the liquid. For water, the accommodation coefficient can vary from 0.001 (condensation in the presence of humid air) to 1 (condensation of pure steam) [55, 56]. Therefore, since the present model deals with pure water vapor condensation, α is assumed to be equal to 1. The heat transfer coefficient at the liquid-vapor interface is the same for all models.

Chavan et al. [23] have solved the heat transfer rate through droplets on substrates at given temperature and constant contact angle by performing two-dimensional numerical simulations of drop growth. In particular, the conduction thermal resistance has been numerically calculated by a finite element method model, replacing the constant temperature boundary condition at the liquid-vapor interface with a convective boundary condition (constant value of h_i). In the Chavan et al. [23] model, the calculation of the heat transfer through a single droplet is based on the evaluation of the droplet Nusselt number (Nu), which can be expressed as a function of the droplet Biot number (with allowed values from 0.1 to 10^5) and the advancing contact angle (with allowed values from 90° and 170°) as follows:

$$Q_d = \frac{\pi r^2 \left(1 - \frac{r_{min}}{r}\right) \Delta T}{\frac{\pi r}{\mathrm{Nu}(\mathrm{Bi}, \theta_{adv})\ \lambda_l \sin\theta_e} + \frac{\delta_{HC}}{\lambda_{HC}\sin^2\theta_e}} \tag{4}$$

where Bi is the Biot number Bi = ($h_i \times r$) / λ_l, (the Biot number as reported by Lethuillier et al. [24] refers to the curvature radius r instead of the base radius r_b of the droplet) which indicates whether the temperatures inside a body vary significantly when a certain thermal gradient is applied to its surface. In order to calculate the Nusselt number, the authors have provided the following expressions (with θ_{adv} and θ_e in radians):

$$\mathrm{Nu} = 3\ \theta_{adv}^{0.65}\ (\mathrm{Bi}\sin\theta_e)^{0.83} + 0.007\ \theta_{adv}^{5.1}\ (\mathrm{Bi}\sin\theta_e)^{-0.23} \quad \text{for} \quad \mathrm{Bi}\sin\theta_e \le 0.5 \tag{5}$$

$$\mathrm{Nu} = 0.29\ \theta_{adv}^{2.24}\ (\mathrm{Bi}\sin\theta_e)^{-0.17} + 3.33\ \theta_{adv}^{-0.3}\ (\mathrm{Bi}\sin\theta_e)^{0.72} \quad \text{for} \quad 0.5 < \mathrm{Bi}\sin\theta_e \le 2 \tag{6}$$

$$\mathrm{Nu} = 5.76\ e^{-0.28\ \theta_{adv}^{0.68}} \ln\left(1 + 5\ (\mathrm{Bi}\sin\theta_e)^{0.82} - 2.79\ (\mathrm{Bi}\sin\theta_e)^{0.83}\right) \quad \text{for} \quad 2 < \mathrm{Bi}\sin\theta_e \le 10^5 \tag{7}$$

Similarly, Lethuillier et al. [24] have recently used a numerical approach to extend the validity range of the single droplet heat transfer model from superhydrophilic to superhydrophobic surfaces, considering the full range of Biot numbers encountered during dropwise condensation. Considering a reference case whose exact analytical solution is known and comparing the results with an independent instrument based on the Monte Carlo method, the authors have refined the mesh in the region of the triple line avoiding simulation lost accuracy as the Biot number increases. The triple line region as demonstrated by Kim et al. [57] is crucial in order to describe the heat transfer during DWC. Both the validity range of contact angles (from 20° to 170°) and Biot number (from 10^{-4} to 10^5) have been increased with respect to the model proposed by Chavan et al. [23].

In the Lethuillier et al. [24] model, the heat transfer rate through a single drop is given by:

$$Q_d = \frac{\pi r^2 \left(1 - \frac{r_{min}}{r}\right) \Delta T}{\frac{\delta_{HC}}{\lambda_{HC}\sin^2\theta_e} + \frac{1}{2h_i(1-\cos\theta_e)} + \frac{\pi r}{\lambda_l} f(\theta_e, \mathrm{Bi})} \tag{8}$$

where:

$$f(\theta_e, \mathrm{Bi}) = \zeta_0\ \zeta_4 \quad \text{for} \quad \mathrm{Bi} \le 10^{-2} \tag{9}$$

$$f(\theta_e, \mathrm{Bi}) = \zeta_0\ [\tanh(\zeta_1 - \log\mathrm{Bi}) - \tanh(\zeta_2 + \zeta_3 \log\mathrm{Bi}) + \zeta_4] \quad \text{for} \quad 10^{-2} < \mathrm{Bi} \le 10^5 \tag{10}$$

$$\zeta_i = \sum_{j=0}^{6} a_{i,j}\ \theta_e^j\ + b_i \tan\frac{\theta_e}{2} \tag{11}$$

For the analytical expressions of the coefficients $a_{i,j}$ and b_i, the reader can refer to the original manuscript by Lethuillier et al. [24]. In the case of surfaces with contact angles above 120°, it would be necessary to add the liquid-solid interfacial thermal resistance developed by Niu et al. [58] to the equation for the heat transfer exchanged by a single droplet. However, as reported by the authors, the contribution of such resistance is important only for superhydrophobic surfaces (contact angles higher than 155°) and high subcooling degrees, while it is negligible in the present case.

The single droplet heat transfer predictions (Q_d) calculated by the Miljkovic et al. [22], Chavan et al. [23] and Lethuillier et al. [24] models are shown in Fig. 2 as a function of the droplet radius. The coating thickness was assumed to be equal to zero ($\delta_{HC} = 0$) in order to exclude the effect of the coating thermal resistance on Q_d. Therefore, the comparison focuses on the different modelling of the droplet conduction resistance and of the vapor-liquid interface resistance proposed by the three models.

As it can be observed in Fig. 2, the models by Lethuillier et al. [24] and Chavan et al. [23] predict nearly the same single droplet heat transfer in the range of contact angles between 90° and 150° Instead, the Miljkovic et al. model [22] provides lower values of Q_d for larger drop sizes compared to the models by Chavan et al. [23] and Lethuillier et al. [24].

Assuming that all the heat transfer during DWC occurs through the droplets, the single drop heat transfer rate (Q_d) can be equated to the condensation rate of vapor at the droplet surface (Eq. (12)) to obtain the droplet growth rate ($G = \mathrm{d}r/\mathrm{d}t$):

$$Q_d = \rho_l\ h_{lv}\ \pi\ r^2 \left(2 - 3\cos\theta_e + \cos^3\theta_e\right) G \tag{12}$$

To calculate the droplet growth rate of each heat transfer model, the

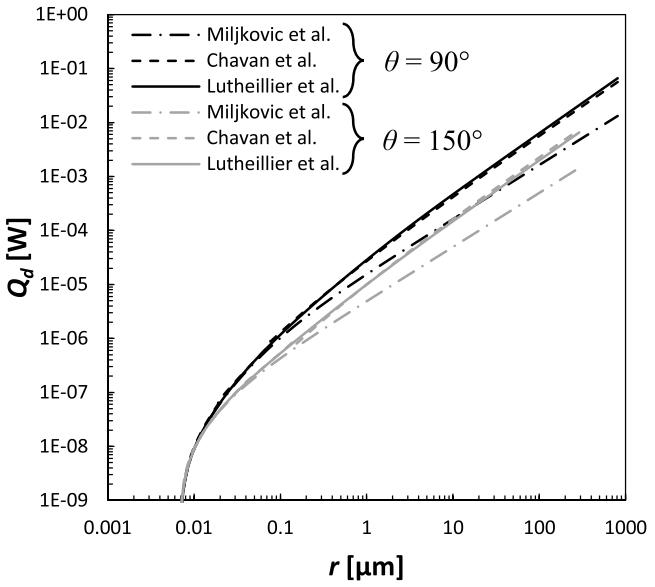

Fig. 2. Comparison of models used to compute the single droplet heat transfer rate, Q_d [22–24] in the present simulations. Two different surface wettability values (90° and 150° contact angles) were considered, under the following thermodynamic conditions: $\Delta T = 3$ K and $T_{sat} = 105$ °C. The coating resistance has been neglected.

expressions of Q_d derived by Miljkovic et al. [22] (Eq. (2)), Chavan et al. [23] (Eq. (4)) and Lethuillier et al. [24] (Eq. (8)) should be substituted into Eq. (12).

2.3. Coalescence

During dropwise condensation, the droplets can also grow by coalescing with neighboring drops. When coalescence occurs, the merging drops are instantly replaced by a new drop with the volume calculated by applying the conservation of the total volume. The resulting drop is placed in the center of mass of the drops involved in the coalescence. According to the instantaneous coalescence hypothesis, the droplet formed by the coalescence of two or more droplets is considered to be mechanically stable instantaneously, without taking into account any oscillations of the interface. There are few studies in the literature that investigate the effect of coalescence dynamics, and they usually focus on the coalescence of only two drops [59,60]. Adhikari and Rattner [59] conducted a numerical simulation of droplet coalescence event by using CFD simulations and they found that considering the droplet dynamics during a coalescence process leads to an increase in the transferred heat flow rate compared against the simplified case of instantaneous coalescence. However, from their research, no information is provided about the heat flux when the number of merging droplets is greater than two. Considering coalescing droplets dynamics in an IBM would also require the simultaneous resolution of the contact line by performing CFD simulations with about 10 droplets coalescing together when using a time step of 10^{-5} s and with a nucleation site density of 5×10^{12} m^{-2}. The criterion for the identification of the droplets that come into contact depends on the surface wettability. In the case of hydrophilic surfaces ($\theta_e < 90°$), the drops merge when their triple lines touch, i.e. when the distance between the mass center of the drops i and j is smaller than the sum of the base radii r_b of the drops:

$$r_{b,i} + r_{b,j} > \sqrt{\left(x_i - x_j\right)^2 + \left(y_i - y_j\right)^2} \tag{13}$$

While, in the case of hydrophobic surfaces ($\theta_e > 90°$), some drops could be hidden under other larger drops. The drops coalesce when the distance between the center of mass of the drops i and j become less than the sum of the curvature radii r of the drops involved in the coalescence. Since the coordinate of a droplet centroid is (x, y, $|r \cos \theta_e|$), the criterion for coalescence in the case of hydrophobic surfaces is:

$$r_i + r_j > \sqrt{\left(x_i - x_j\right)^2 + \left(y_i - y_j\right)^2 + \left(r_i - r_j\right)^2 \cos^2\theta_e} \tag{14}$$

The coalescence is considered instantaneous, i.e. during the numerical simulation, the drops involved in the coalescence are replaced with a droplet of size and position different from the parent drops within a time step. It is interesting to note that, if the resulting drop touches other drops (cascading coalescence), the algorithm of coalescence can be repeated until the end of the coalescence events as shown in Fig 1. However, in order to approximate the evolution of the real coalescence between multiple drops, the function for coalescence is called only once. In this way, especially for large droplets, the coalescence process lasts a few time steps. It has been demonstrated that, as long as the time step is sufficiently small, the effect of the cascading coalescence can be neglected [39]. While, in terms of computational efficiency, the program becomes about 50 % faster.

The determination of the mutual distances between drops is the most onerous process from the computational point of view. Therefore, to improve the efficiency of the present IBM, C code has been coupled with OpenMP library in order to parallelize the calculation over multiple cores/threads. For example, in the case of 10^5 drops in the simulation domain, the present method (run on 32 threads) leads to an improvement of about 1500 times in terms of computational efficiency (defined as the ratio between the time simulated and the time required to simulate it, Eq. (21)) compared to the single core MATLAB® program. The use of parallel computing constitutes one of the main differences between the present IBM and the IBMs proposed in the literature. It should be noted that, using the present IBM, it is possible to simulate more than 10^7 drops while maintaining the computational times not prohibitive. Further information will be provided in Section 3.

2.4. Departure and sliding

During DWC, the droplets grow from the nucleation radius (r_{min}) until the departing radius (r_{max}). The latter derives from a force balance between adhesion forces and external forces which induce the droplet movement (e.g., drag and gravity). On a vertically oriented surface (as in the case of the present experiments, see Section 4.1) both the gravitational force and the shear stress of the vapor act in the same direction, improving the sweeping process and the renewal of the underneath surface. In recent works [30,48,61], the present authors proposed a method for modeling the effect of vapor velocity on the droplet departing radius that accounts for the drag force into the force balance equation.

The adhesion force for a circular-shaped drop is calculated by integration along the drop contour and it can be expressed as follows:

$$F_{ad} = 2\ k_c\ \sigma \sin\theta_e (\cos\theta_{rec} - \cos\theta_{adv}) r \tag{15}$$

where k_c is the retention factor, and g is the gravitational acceleration. The retention factor depends on the contour of the droplet. For a circular-shaped drop, it is equal to $2/\pi$ [62].

The gravity force depends on the volume of the drop and on the inclination of the surface. For a vertically oriented surface, the gravity force is given by:

$$F_g = \frac{\pi}{3}\left(2 - 3\cos\theta_e + \cos^3\theta_e\right)\ \rho_l\ g\ r^3 \tag{16}$$

By equating Eqs. (15) and 16, the classical formulation for the droplet departing radius in the absence of vapor velocity can be obtained.

According to formulation proposed by Batchelor [63], the drag force acting on the droplet can be expressed as follows:

$$F_{dr} = \frac{1}{2}\,\rho_v\, v_v^2\, C_d\, r^2(\theta_e - \sin\theta_e\cos\theta_e) \tag{17}$$

where C_d is the drag coefficient and θ_e is the equilibrium contact angle expressed in radians. By means of numerical simulations, the authors [48] found that the drag coefficient can be evaluated using two dimensionless groups: the droplet Reynolds number (Re_d) and the ratio between the channel height and the drop height (L_{ch}/l_d).

$$C_d = 5.6053\left[\left(\frac{L_{ch}}{l_d}\right)^{-4/3} \mathrm{Re}_d^{-1/6}\right] + 0.1754 \tag{18}$$

Therefore, to account for the effect of vapor velocity on the departing radius, the adhesion force (Eq. (15)) must be equated to the sum of the gravity force and drag force (Eqs. (16), (17)) as shown below:

$$F_{ad}(r_{max}) = F_g(r_{max}) + F_{dr}(r_{max}) \tag{19}$$

As stated in [48], the present method for the evaluation of the droplet departing radius requires an iterative procedure.

Another fundamental aspect that differentiates the present IBM from those of Stevens et al. [39] and Lethuillier et al. [38] concerns the droplet sliding velocity. Instead of considering a fixed sliding velocity (as assumed in [38,39]), the present model can account for variable sliding velocity due to a non-zero droplet sliding acceleration. In fact, as observed in [30,48], the droplets motion during DWC is uniformly accelerated in the case of a vertically oriented surface. The equation used to calculate the new position of the center of mass of a sliding droplet at each simulated time step is given by:

$$\Delta y = a\cdot(t - t_0)\,\Delta\tau + \frac{1}{2}a\,(\Delta\tau)^2 \tag{20}$$

where a is the droplet acceleration, $\Delta\tau$ is the simulation time step, t_0 is the initial time of the sliding process for the current droplet and t is the current simulation time. In the present work, a is fixed according to the experimental data obtained by Tancon et al. [48],

2.5. Numerical procedure

The present IBM requires several input parameters to perform DWC simulations. At each time step, the IBM calculates the heat flux transferred by the surface and the drop-size distribution. The instantaneous outputs can be averaged over the entire simulation to obtain the time-averaged results.

The model inputs are divided into thermodynamic and geometrical input quantities and numerical parameters. The following quantities belong to the first group: properties of the hydrophobic layer such as thermal conductivity (λ_{HC}) and thickness (δ_{HC}), advancing (θ_{adv}) and receding (θ_{rec}) contact angles, operating conditions such as saturation temperature (T_{sat}), surface subcooling (ΔT), vapor velocity (v_v) and surface orientation. The departing radius (r_{max}) is obtained as discussed in Section 2.4. Unless otherwise indicated, all the results presented in this study are based on the same parameters presented in Table 1. Water is used as the working fluid, and its thermodynamic and transport properties are calculated using REFPROP v10 [64].

Table 1
Input parameters for dropwise condensation simulations.

Parameter	Value
Saturated vapor temperature [°C]	108
Subcooling degree [K]	3.5
Vapor velocity [m s^{-1}]	13.8
Coating thickness [nm]	380
Thermal conductivity of coating [W m^{-1} K^{-1}]	0.25
Contact angle hysteresis [°]	20° ±4°
Advancing contact angle [°]	87° ± 3°
Receding contact angle [°]	67° ± 2°
Time step [s]	From 10^{-6} to 10^{-3}
Nucleation sites density [m^{-2}]	From 10^9 to 5×10^{12}

The numerical input parameters are the parameters required to ensure the proper operation of the IBM: nucleation site density (N_s), time step ($\Delta\tau$), extension of the computational domain, and selected heat transfer model (Miljkovic et al. [22], Chavan et al. [23] or Lethuillier et al. [24]). With regards to the computational domain, the time step, and the number of nucleation sites, an accurate analysis of their effects on the results of the simulations (overall heat flux and drop-size distribution) has been reported in Section 3.2. The range of time step and nucleation sites density used in the present simulations are summarized in Table 1. The effect of the single droplet heat transfer model on the dropwise condensation heat flux predicted by the IBM was studied considering a departing radius of 65 μm, a nucleation sites density of 2×10^{10} m^{-2}, and a time step of 10^{-5} s. The results show that the Chavan et al. [19] and Lethuillier et al. [20] models give similar predictions, with a deviation in the calculated heat flux of about 8 % ($q_{d,\ Lethuillier} = 407$ kW m^{-2}, $q_{d,\ Chavan} = 374$ kW m^{-2}), while the Miljkovic et al. [18] predicts values considerably lower compared to Lethuillier et al. [20] and Chavan et al. [19] ($q_{d,\ Miljkovic} = 219$ kW m^{-2}). As discussed in Section 2.2, the difference among the models is related to the definition of the droplet conduction resistance. In the present work, the Lethuillier et al. [24] model is used for the evaluation of the heat transfer through a single droplet as it is the most up-to-date model in the literature, suitable to accounts for the entire wettability range considered in the present work.

Unless otherwise indicated, the simulations were performed considering a nucleation sites density of 5×10^{12} m^{-2}, a time step of 10^{-5} s (a detailed analysis of the effect of the time step is carried out in Section 3.2 - 3.3) and a simulated domain equal to 1.5 × 1.5 mm^2. The reproducibility of the results was verified in terms of overall heat flux by repeating the calculations for different randomly distributed nucleation sites positions. For each simulation, a statistical analysis was performed using the Ripley L function [65], evaluating whether the sites were regularly distributed over the surface, from which discrepancies of less than 1 % were obtained once the simulation reached the steady-state conditions.

3. Results and discussions

In this section, the present IBM is compared with the most up-to-date IBMs of the literature in terms of computational efficiency. Then, the parameters of the present model (simulation domain, time step, and duration of the simulation) are optimized to improve the efficiency of the whole IBM without losing precision in the calculated heat flux and drop-size distribution. After the discussion on the time step of the simulation, a comparison between PBM (population-based models) and the present IBM (individual-based model) is presented both in terms of drop-size distribution and total heat flux. Finally, the effect of the acceleration of the sliding droplets on the drop-size distribution is discussed.

3.1. Overview of the present IBM

As shown by Parin et al. [7], for a direct comparison with the experimental data obtained during DWC of steam, a high nucleation sites density (between 10^{12} and 10^{13} m^{-2}) should be considered in the heat transfer model. In a computational domain of 1.5 × 1.5 mm^2, with $N_s = 10^{13}$ m^{-2}, the number of drops to be simulated is about 2×10^7 drops (further detail are reported in Section 4). The huge number of drops requires to optimize the input parameters for the numerical simulation in order to reduce the computational effort as much as possible. For this reason, as described in Section 2, the hybrid use of the MATLAB® and C codes was implemented. The C code was used to perform the most onerous functions from the computational point of view, while MATLAB® was used as the main code for both saving/-retrieving and displaying the results. It was observed that the same

functions performed using the hybrid MATLAB® and C code leads to an improvement of about 500 times as compared to the use of MATLAB® alone [66]. Furthermore, in the present model, the C code has been enhanced using the OpenMP library which distributes the most complex calculations across multiple cores/threads.

For the simulations, a machine with CPU AMD EPYC ™ 7282 16C/32T and 128 GB of RAM was used. The use of the OpenMP library allows the simultaneous execution of the C code on multiple cores of the same processor in order to increase the computing performance. The parallelization on 32 threads significantly reduces the simulation time up to about 1500 times when the number of drops is 10^5 as compared to the single-core program. To compare the performance of the present IBM with those in the literature, the computational efficiency (ε_{sim}) as proposed by Hu et al. [44] can be evaluated:

$$\varepsilon_{sim} = \frac{\Delta t_{real}}{\Delta t_{sim}} \tag{21}$$

where Δt_{real} is the simulated real-time and Δt_{sim} is the time required to run the simulation. Hence, the computational efficiency is defined as the ratio of the real time interval of simulated DWC to the computation time required for the simulation of that time interval.

In Fig. 3, the computational efficiency of the present IBM (both the single core MATLAB® and the multi-thread MATLAB® & C configurations) is plotted against the number of simulated drops. For comparison, Fig. 3 also shows the computational efficiencies of the IBMs by Hu et al. [44], Meng et al. [41], and Burnside and Hadi [40]. The computational efficiency of the present IBM is much higher as compared to the others model in the literature, and the advantage improves as the number of drops on the surface increases. The higher the efficiency, the smaller the time required to simulate a given time interval. For example, with a time step $\Delta\tau = 10^{-3}$ s and a simulation time $\Delta t_{real} = 1$ s, the present IBM takes 11 s to simulate the case with 2×10^5 drops, while the IBM of Hu et al. [44] takes 2 min. Instead, to simulate 10^7 drops, the present IBM takes 8 min, while the IBM of Hu et al. [44] takes 4.5 h.

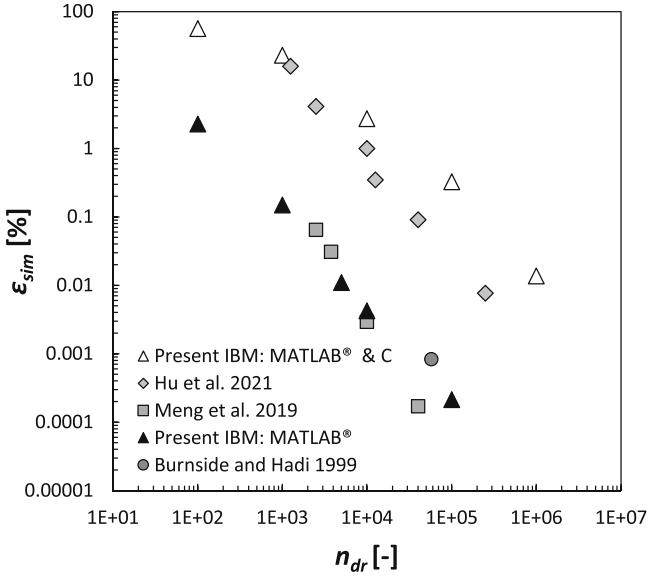

Fig. 3. Computational efficiency (Eq. (21)) plotted vs number of droplets: comparison between the present IBM (individual based model) based on parallel computing developed in MATLAB® coupled with C, the same IBM developed in single-core MATLAB®, and the simulations proposed in the literature by Hu et al. [44], Meng et al. [41], and Burnside and Hadi [40]. Unless specified, it should be noted the simulations have been performed with a time step of 10^{-3} s as proposed by Hu et al. [44].

3.2. Optimization of the input parameters

In order to optimize the calculation times, a preliminary study was carried out to evaluate the effect of the main control parameters (i.e. the parameters that can be tuned in the simulations) on the calculated heat flux and the computational efficiency. Different combinations of time step, area of the numerical domain, and simulated time were studied, and the results were compared against a reference case. For all the simulations, the input parameters are those reported in Table 1, while the nucleation sites density is 2×10^{10} m^{-2} and the departing radius is $r_{max} = 65$ μm. The reference simulation was run with a time step of 10^{-5} s, a simulation domain of 0.25 mm^2 (about 20 times larger than the area occupied by a drop with the maximum radius of $r_{max} = 65$ μm), and a simulated time of 2 s. As discussed in Section 2.3, since the effect of cascading coalescences on the simulation results is negligible, the algorithm of coalescence is performed only once at each time step. In this way, the simulations become about 50 % faster.

The results of the analysis are shown in Table 2. The results show that the heat flux is sensitive to the time step ($\Delta\tau$). Considering $\Delta\tau = 10^{-3}$ s, the calculated heat flux is about 13 % lower than compared to the reference case ($q_{DWC} = 396$ kW m^{-2}). On the other hand, the computational efficiency improves by about 60 times but, unfortunately, such a long time step does not allow to adequately characterize the drop-size distribution of small drops (as shown in Section 3.3). In fact, if the growth rate is calculated by Eq. (8) and Eq. (12) using a time step of 10^{-3} s, 4 iterations are sufficient for the drops to grow from r_{min} to r_e. Since the IBM calculates the droplet size over time as a frame sequence, the resulting average drop-size distribution obtained results to be scattered as shown in Fig. 5.

The reduction of the computational domain can be a strategy to reduce the number of drops to be simulated, improving the computational efficiency. In particular, the results show that, for a 90 % area reduction, the variation of the heat flux remains below 10 %, while the calculation time is reduced by 5 times compared to the reference case. Finally, the reduction of the simulation time does not appear to affect both the heat flux and the efficiency of the simulation, while it does affect the number of sliding events and the overall computational time. If the simulation lasts less than the time required to observe a sliding event, no conclusion can be drawn on the DWC phenomenon as the quasi steady-state is not reached. In the present analysis, for a simulated time of 2 s, a minimum of 10 sliding events were observed, while, for a simulated time of 0.1 s, at least one sliding event occurred. The 14th configuration was performed starting from the results of the previous simulations. The parameters are $\Delta\tau = 5 \times 10^{-5}$ s, $A = 0.01875$ mm^2 and a simulation time $\Delta t = 0.1$ s. The simulation showed deviation of the heat flux by only 1.9 % compared to the reference case, but the computation efficiency was improved by about 21 times. For this combination of control parameters, a complete cycle of the DWC process from nucleation to sliding and subsequent renucleation was simulated.

In the following analyses, it is assumed that the optimized control parameters (such as the time step, the computational domain edge to the maximum droplet dimension ratio, and the simulation time that includes at least one sliding event) found for the small-scale case remains the same even increasing the maximum radius (from 65 μm to 0.7 mm) and the number of nucleation sites ($N_s = 5 \times 10^{12}$ m^{-2}). However, it has been observed that the choice of the time step is also related to the number of nucleation sites. The larger N_s, the smaller the time step required to accurately approximate the distribution of small drops. Therefore, a time step $\Delta\tau = 10^{-5}$ s has been chosen to have a good discretization of the distribution in the whole radii range. Clearly, since the simulation time and the computational domain are related to the maximum radius, if the maximum radius increases, both the time to simulate a complete cycle of DWC (from nucleation to sliding and r_e nucleation) and the computational domain must be increased. From the results in Table 2, it was found that the minimum side of the square computational domain must be 5 % higher than the diameter of the

Table 2
Configurations of the main control parameters in the simulation: the results (computational efficiency ε_{sim} and heat flux q_{DWC}) of the different configurations obtained by varying the computational domain, time step, and duration of the simulation are reported as the ratio to the reference case.

	$\Delta\tau$ [μs]	Time [s]	l_x [mm]	A [mm^2]	$n_{droplets}$ [-]	ε_{sim}	q_{DWC}
Reference case	10	2	0.5	0.25	5000	0.025 %	396 kW m^{-2}
		Varied parameters				% variation with respect to the reference case	
1	**20**	2	0.5	0.25	5000	160%	0.4%
2	**50**	2	0.5	0.25	5000	500%	-0.8%
3	**100**	2	0.5	0.25	5000	1018%	-1.6%
4	**1000**	2	0.5	0.25	5000	6157%	-12.8%
5	10	**1**	0.5	0.25	5000	-0.10%	0.2%
6	10	**0.5**	0.5	0.25	5000	-1.60%	-0.1%
7	10	**0.25**	0.5	0.25	5000	-6.70%	-0.6%
8	10	**0.1**	0.5	0.25	5000	-8.40%	-1.5%
9	10	1	0.35	**0.125**	2500	158%	1.0%
10	10	1	0.25	**0.0625**	1250	403%	2.4%
11	10	1	0.16	**0.025**	500	802%	10.3%
12	10	1	0.15	**0.0225**	450	565%	7.8%
13	10	1	0.14	**0.01875**	375	608%	5.3%
14	**50**	**0.1**	0.14	**0.01875**	375	1976%	1.9%

departing drops ($2 \times r_{max}$).

Fig. 4 shows the evolution of the droplet population in the case of DWC of saturated vapor on a vertically oriented hydrophobic surface. The simulation shows all the stages of the DWC: the formation of new drops on the nucleation sites, the growth by simultaneous action of direct condensation and coalesce with neighbour droplets, the sweeping of the surface due to sliding drops, and the repetition of the mechanisms.

3.3. Droplet population and heat flux calculation

According to the traditional statistical models (PBMs) [19–22], the time-averaged drop-size distribution is a fundamental parameter for the calculation of the overall heat flux transferred during DWC (q_{DWC}). By knowing the heat transferred through a single droplet (Section 2.2) and the average drop-size distribution, the overall heat flux can be calculated as follows:

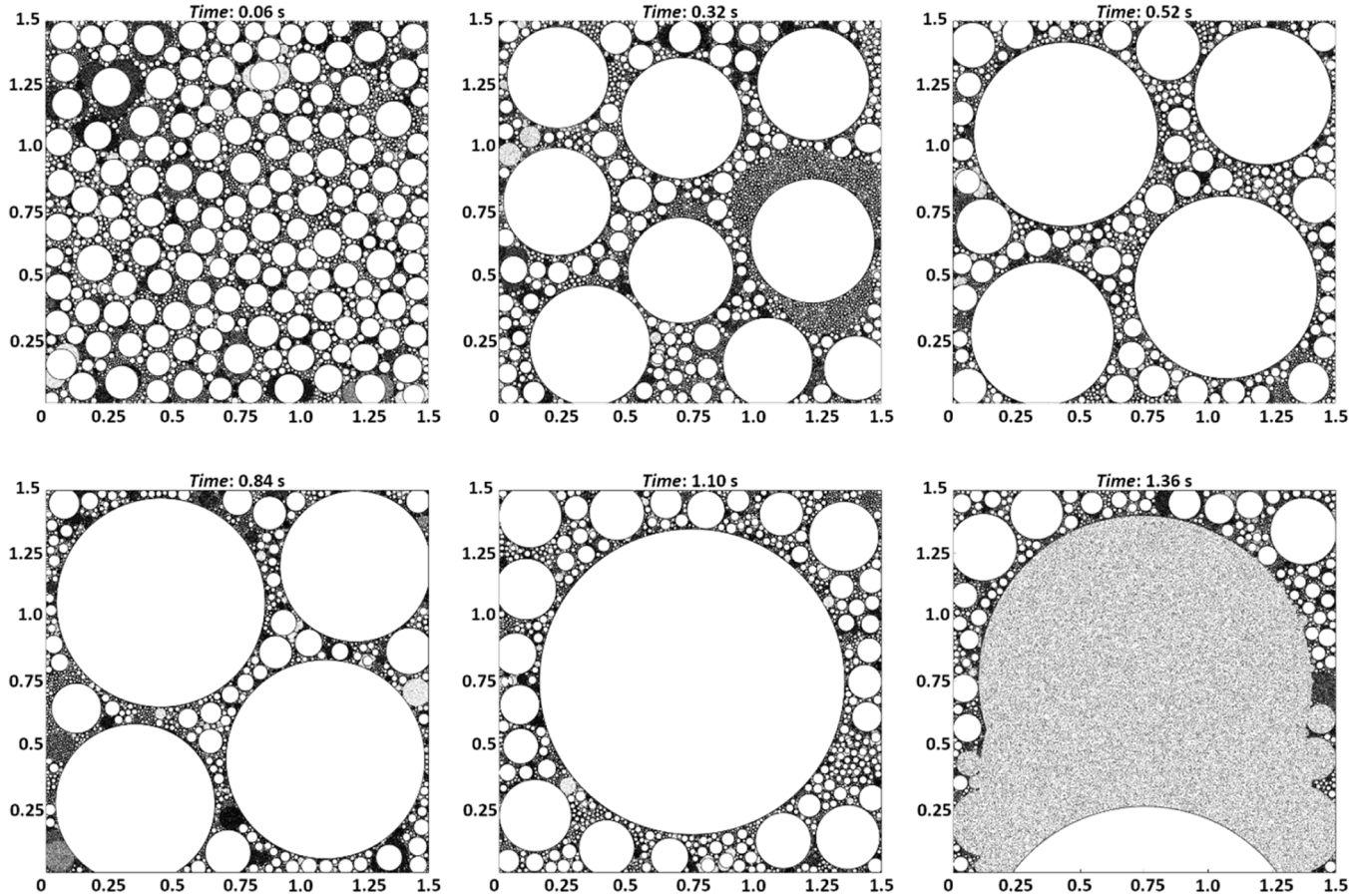

Fig. 4. Visualization of the nucleation, growth and sliding of droplets during DWC of pure steam. Simulation parameters: $l_x = l_y = 1.5$ mm, $N_s = 5 \times 10^{12}$ m^{-2}, $\Delta\tau = 10^{-5}$ s, $\Delta t_{sim} = 1.5$ s and, $a = 2.6$ m s^{-1}.

$$q = \int_{r_{min}}^{r_e} Q_d(r)\ n(r)\ \mathrm{d}r + \int_{r_e}^{r_{max}} Q_d(r)\ N(r)\ \mathrm{d}r \tag{22}$$

$N(r)$ and $n(r)$ are the drop-size density function of large and small droplets, respectively. The integral is divided into two parts depending on droplet growth mechanism. Small droplets ($r_{min} \le r < r_e$) grow only by direct condensation, while large droplets ($r_e \le r \le r_{max}$) grow mainly by coalescence with neighbouring droplets and marginally by direct condensation. In the literature, it is well known that the average drop-size distribution on the condensing surface remains constant over time once the steady-state conditions are reached [19]. The two droplet populations are separated by the so-called effective radius (r_e) which depends on the number of the nucleation sites. The Kim and Kim's model [21] assumes that the drops are arranged in a square lattice, while Miljkovic et al. [22] assume that drops are distributed following a Poisson distribution. Stevens et al. [39] showed that a Poisson distribution accurately reflects the distribution of drops during condensation over a uniform wettability surface. So, under the hypothesis that the nucleation sites are randomly distributed [22] over the surface, r_e is given by:

$$r_e = \frac{1}{4\sqrt{N_s}} \tag{23}$$

where N_s is the number of nucleation sites per unit of condensation surface.

To describe the distribution of large drops $N(r)$, the semi-empirical law introduced by Le Fevre and Rose [27] is generally used. Subsequently, Rose and Glicksman [29] derived an analytic expression for this law in which the only two variables are the drop radius r and the departing radius r_{max}, and it is given by:

$$N(r) = \frac{1}{3\pi\ r_{\max}\ r^2}\left(\frac{r}{r_{\max}}\right)^{-2\ /3} \tag{24}$$

On the other hand, as proposed by Tanaka in his works [25,26], the distribution of the small drops can be calculated from the resolution of the population balance theory. All the PBMs in the literature [20–22] use the following equation to describe the drop-size distribution of small drops:

$$n(r) = N(r_e)\frac{r(r_e - r_{min})(A_2 r + A_3)}{r_e(r - r_{min})(A_2 r_e + A_3)} e^{B_1 + B_2} \tag{25}$$

Since the coefficients A_2, A_3, B_1 and B_2 depends on the formulation of the heat flow rate exchanged by a single drop, only few authors [20–22] have proposed an analytical expression for the population of small drops. Among the main works in the literature, it is worth to mention that, based on their model for the heat transfer through a single droplet, Miljkovic et al. [22] obtained analytical expressions of coefficients A_2, A_3, B_1 and B_2. By coupling Eq. (22) with the distributions of small droplets (Eq. (25)) and large drops (Eq. (24)) and with the expressions for the heat flux exchanged by a single drop (Eqs. (2), (4) and (8)), the overall heat flux transferred during DWC can be analytically solved.

In the case of IBMs, the total heat flux can be easily calculated by knowing the dimension of each drop within the surface. Then the instantaneous heat flux is calculated as:

$$\widetilde{q} = \frac{1}{A}\cdot\sum_{i=0}^{n} Q_{d,i} \tag{26}$$

where n is the number of drops over the surface at each time step. The instantaneous heat flux fluctuates periodically due to the evolution of the growth, coalescence and sliding mechanisms. As shown in Fig. 8b, the instantaneous heat flux reaches a minimum value when the computational domain is mostly occupied by large droplets, while it shows a maximum once the surface is renewed. The mean heat flux q given by the IBM can be obtained by averaging the instantaneous heat fluxes values ($\widetilde{q}$) over the simulation. With the development of complex single droplet heat transfer models, performing numerical simulations, which simulate the growth by both coalescence and direct condensation, allows the study of the drop-size distribution. In order to evaluate the drop-size distribution by numerical simulation (IBM), the first step is to divide the entire range of radii (from r_{min} to r_{max}) in a series of intervals, and then count how many drops fall into each interval. In order to detect the underlying shape of the distribution, the bins must be adjacent (non-overlapping) and of equal logarithmic size. The drop-size distribution is obtained by dividing the histogram (calculated by assigning each droplet into the proper radius interval) by the computational domain area and the number of simulated time instants. Fig. 5a shows the droplet growth rate calculated by coupling Eqs. (12) and (8) (Lethuillier et al. [24] model) as the time step varies from 10^{-6} to 10^{-3} s. The droplet growth rate strongly depends on the time step. Since the function of the growth rate in the radii ranging between 0.005 and 0.02 μm undergoes a strong variation in slope, the growth of the drops in that interval is well approximated only if the time step is lower than 10^{-5} s. For time steps higher than 10^{-4} s, the growth rate of the small drops ($r < r_e$) is heavily underestimated compared to the growth rate calculated with a time step lower than 10^{-5} s. For example, considering a time step 10^{-3} s, a droplet with a radius between 0.005 and 0.02 μm increases its size up to 12 times between two consecutive time steps (Fig. 5a). Consequently, a time step greater than 10^{-4} s, which does not allow to well describe the growth of small drops, leads to a wrong shape of the drop-size density function (Fig. 5b), underestimating the calculated condensation heat flux (Table 2). The results show that the use of time step higher than 10^{-4} s has benefits from the computational point of view but is not suitable for the evaluation of the drop-size distribution.

In Table 3, the models considered in the present study are summarized. In particular, Lethuillier et al. [24], Chavan et al. [23], and Miljkovic et al. [22] have developed a model for the heat flux transferred by a single drop. Among these models, only Miljkovic et al. [22] solved the population balance theory to obtain an analytical expression for the distribution of small drops $n(r)$. Instead, the Meng et al. [41], Hu et al. [44], Burnside and Hadi [40] models and the present model evaluates the drop-size distribution by simulating the DWC process through an IBM.

Using the present IBM, it is now possible to numerically study the dynamics of the drops and thus obtain the drop-size density and the overall heat transferred during DWC. Fig. 6a shows the comparison between the heat flux calculated by the present IBM and the one calculated by the combination of Eqs. (2), (4), (8), (22), (24), (25) for different values of nucleation sites density. The IBM simulations as well as the PBM calculations were performed at the conditions listed in Table 1, considering the same computational domain ($A = 1.5 \times 1.5$ mm^2), departing radius ($r_{max} = 0.7$ mm), time step ($\Delta\tau = 10^{-5}$ s) and single drop heat transfer model (Lethuillier et al. [24]).

As the number of nucleation sites increases, the heat flux predicted by the two approaches, PBM and IBM, also increases. However, the heat flux predicted by the PBMs at varying N_s follows a different trend compared to the one predicted by the IBM (dotted black line). Applying Eqs. (22), (24), (25) with the aforementioned models for the evaluation of the heat flow rate through a single drop [22–24], the resulting heat flux varies (according to the selected heat transfer model for the droplet) but the trend of heat flux versus nucleation sites density remains constant. In particular, when considering PBMs, two different slopes of the curve can be identified: one for droplets radii between 10^9 and 10^{11} m^{-2} and another one (much lower) for droplets radii between 10^{11} and 2×10^{15} m^{-2}. Instead, the heat flux predicted by the IBM is found to follow a linear trend in the graph of Fig. 6a at least for N_s range between 10^9 and 5×10^{12} m^{-2}. It must be noted that the simulations are limited to $N_s = 5 \times 10^{12}$ m^{-2} to maintain a reasonable computational time. For $N_s = 2 \times 10^{15}$ m^{-2}, r_e calculated by Eq. (23) becomes equal to r_{min} and thus the small droplets population (characterized by droplets growth by direct vapour condensation without coalescence) disappears. Under these

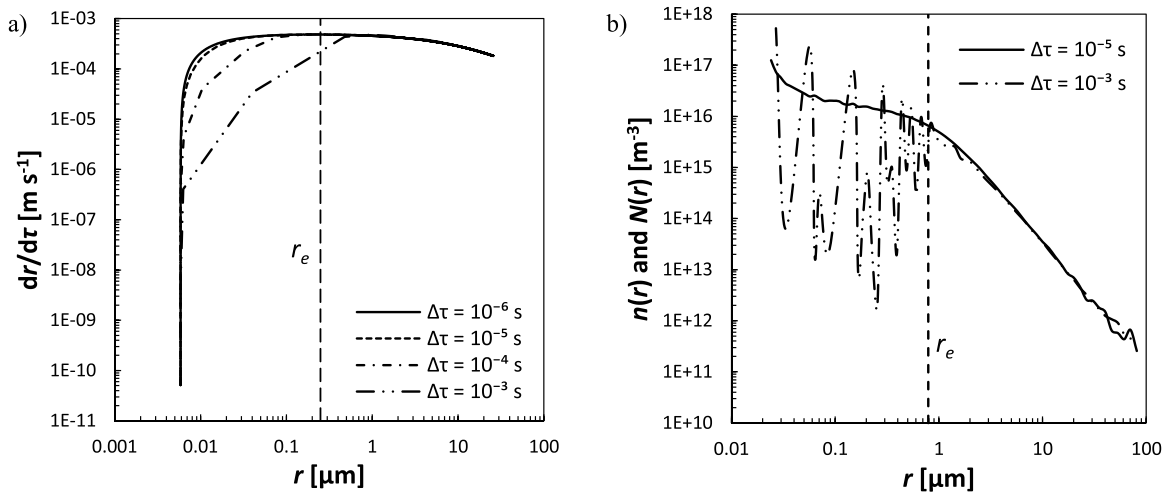

Fig. 5. (a) Droplet growth rate $dr/d\tau$ obtained from the Lethuillier et al. [24] model using different time steps (from $\Delta\tau = 10^{-6}$ s to $\Delta\tau = 10^{-3}$ s). (b) Drop-size distribution obtained from the numerical simulation performed at two different time steps 10^{-5} s and 10^{-3} s. The equivalent radius r_e is calculated as proposed by Miljkovic et al. [22].

Table 3
List of papers available in the literature in which the authors have developed a single drop heat transfer model, solved the PBM or developed an IBM.

	Q_d model	$n(r)$ by PBM	IBM	Q_d used in IBM
Lethuillier et al. [24]	x			
Chavan et al. [23]	x			
Miljkovic et al. [22]	x	x		
Present work			x	Lethuillier et al. [24]
Hu et al. [44]			x	Miljkovic et al. [22]
Meng et al. [41]			x	Miljkovic et al. [22]
Burnside and Hadi [40]			x	Le Fevre and Rose [27]

conditions, the first integral in Eq. (22) is equal to zero and the droplet population from r_{min} to r_{max} can be described using only the equation by Le Fevre and Rose [27] (Eq. (24)).

This remark can be confirmed looking at Fig. 6b. For $N_s = 10^9$ m^{-2} and $N_s = 10^{11}$ m^{-2}, the drop-size distribution of large drops obtained by present IBM is well fitted by the Le Fevre and Rose [27] model. Increasing N_s, the effective radius r_e (Eq. (23)) would tend to r_{min} and, therefore, the whole drop-size distribution from r_{min} to r_{max} (Eq. (24)) could be described only by the Le Fevre and Rose [27] model (Eq. (24)), neglecting the small droplet population (obtained from the population balance model). In particular, for $r_e = r_{min}$, the drop-size distribution predicted by the present IBM is expected to exactly match the one predicted by Le Fevre and Rose [27], making the total heat flux calculated by the present IBM equal to the value obtained by solving the integral (Eq. (22)) with only the Le Fevre and Rose distribution from r_{min} to r_{max} (Eq. (24)). In fact, extending the dotted black line (which interpolates the present IBM data of Fig. 6a) up to $N_s = 2 \times 10^{15}$ m^{-2}, it results that the IBM extrapolated line (dotted black) and the PBM line (dashed grey, calculated using Lethuillier et al. [24] model) provide the same value of DWC heat flux. This result confirms the linear trend of the heat flux obtained by the present IBM at varying N_s as reported in Fig. 6a.

In Fig. 6b, the drop-size distributions calculated using the PBM proposed by Miljkovic et al. [22] (Eqs. (22), (24), (25)) at varying nucleation sites density ($N_s = 10^9$, 10^{11}, 2×10^{15} m^{-2}) and the distribution obtained by the present IBM for $N_s = 10^9$ m^{-2} and $N_s = 10^{11}$ m^{-2} are compared for the condition listed in Table 1. Both the PBM and IBM

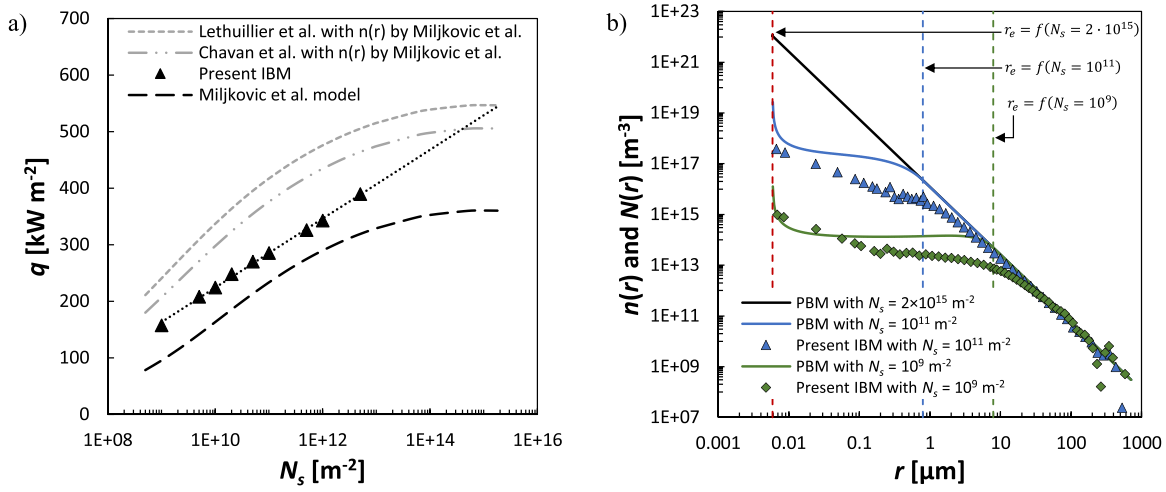

Fig. 6. (a) Average heat flux versus number of nucleation sites obtained from the present IBM ($A = 1.5 \times 1.5$ mm^2, $\Delta\tau = 10^{-5}$ s, other parameters as listed in Table 1) and compared with the theoretical models by Lethuillier et al. [24], Chavan et al. [23], and Miljkovic et al. [22]. Chavan et al. [23] and Lethuillier et al. [24] models are run using the drop-size distribution proposed by Miljkovic et al. [22]. b) The drop-size distributions for small $n(r)$ and large $N(r)$ droplets calculated by the present IBM (dots) and by PBM of Miljkovic et al. [22] (solid lines) when varying the number of nucleation sites N_s.

are solved using the Lethuillier et al. [24] model for the heat transfer through a single droplet. The distribution obtained from the IBM simulation is in good agreement with the large droplet population given by Eq. (24). Instead, as also observed by Lethuillier et al. [38], the drop-size distribution of small drops obtained from the IBM follows a different trend than that obtained by solving the population balance theory. In particular, the distribution predicted by the PBM overestimates the number of drops in the area close r_e. Since these small drops are responsible for most of the heat transfer, the total heat flux is strongly influenced by the choice of the calculation approach (PBM or IBM). This result was experimentally observed by Tancon et al. [15] during dropwise condensation of humid air. Since the number of nucleation sites in the presence of humid air is reduced by about 4 orders of magnitude compared to saturated steam, a portion of the small droplet population (with $r < r_e$) can be experimentally evaluated. The authors [15] observed that close to r_e (calculated with Eq. (23)) the PBM overestimates the number of drops with respect to the experimental data. In the case of the analytical model proposed by Miljkovic et al. [22] (Eq. (2) with Eqs. (22) and (25)), the total heat flux is underestimated. This is because conduction through the drop is a function of both the contact angle and the Biot number. In fact, the more recent models by Chavan et al. [23] (Eq. (4)) and Lethuillier et al. [24] (Eq. (8)) coupled with the droplet distributions proposed by Miljkovic et al. [22] lead to higher values of heat flux.

As shown through ad hoc numerical simulations in Section 3.1, Lethuillier et al. [24] leads to higher heat flux values compared to Chavan et al. [23]. This result is also obtained from the resolution of the PBM. In fact, the application of Eqs. (22) and 25 to the model of Chavan et al. [23] overestimates the total heat flux by about 20 % as compared to the results of the simulation. Instead, for the model of Lethuillier et al. [24] combined with the distribution of the drops that obtained from Eqs. (22) and (25), the heat flux is overestimated by 30 % with respect to the numerical case ($N_s = 5 \times 10^{12}$ m^{-2}). Hence, the present IBM can be an excellent tool to study the behaviour of the small drop population during DWC, reducing the uncertainty given by the resolution of the PBM. In particular, since the IBM does not require an analytical model for the drop-size distribution, it can be used to directly compare different single drop heat transfer models with experimental data. First of all, the possible limits of the current IBM are due to the single-droplet heat transfer model adopted for the simulations. The model proposed by Lethuillier et al. [24] allows the calculation of the heat flow rate exchanged by a single droplet when the contact angle is between 20° and 170°, the surface is flat (without micro/nanostructure), and the Biot number is between 10^{-4} and 10^{5}, thus expanding the applicability limits of previous droplet-grow models [21–23]. However, it is important to note that the Lethuillier et al. [24] model has not been assessed against DWC experimental data because the validation procedure requires the use of an IBM for the calculation of the real droplet distribution. It must be pointed out that, in addition to the aforementioned limits, there are other hypothesis in the present IBM that are necessary to maintain acceptable the computational time. In particular, it is assumed that droplets nucleation in correspondence of preferred sites occurs instantaneously as soon as the surface is renewed, and that also coalescences among droplets can be considered instantaneous events. Depending on the size of coalescing droplets, the assumption of instantaneous coalescence, as highlighted by Adhikari and Rattner [59], could lead to an underestimation of the total heat flux.

3.4. Effect of surface length on droplet population and HTC

The present IBM can predict both the heat flux and the drop-size distribution (Sections. 3.1 and 3.2). In this Section, the developed model is used to study the drop-size distribution and the HTC during DWC upon different portions of area along the vertical condensing surface (named upper, central and lower areas) in the case of gravity and steam acting in the same direction. As firstly discussed by Rose [19], the drop-size distribution should not be affected by the position along the sample. Later, several authors such as Lethuillier et al. [38], with their mathematical models, confirmed that the drop-size distribution is not affected by the sliding drops. Nevertheless, in those IBM models, the drops are assumed to slide with a constant velocity and furthermore small condensation areas with a square shape are often considered. Instead, if considering a rectangular condensation area with the longer edge oriented in the direction of the gravity force, sliding droplets coming from the upper part of the sample can affect the distribution of droplets on the lower part of the sample. The objective of the present Section is precisely to investigate this phenomenon. As observed by Parin et al. [7] and Tancon et al. [48] on a sample with rectangular area of 20 × 50 mm^2, only the drops growing in the upper part of the sample have the time to reach the departing size, while the drops in the lower area cannot reach the maximum size due to the falling drops from the upper region. In addition, the droplets slide with a certain acceleration (as shown in Tancon et al. [48]) that depends on the force balance between gravity, vapor drag force, adhesion, and viscous forces. Therefore, the droplet population is expected to vary along the sample. The present IBM can account for a non-zero acceleration of the sliding droplets and, thus, can be used to investigate the effect of the sliding drops on the distribution and HTC along a vertically oriented surface.

Aiming at studying the drop-size distribution and the heat flux in different positions along the condensation surface, a computational domain with a high aspect ratio (equal to 25) is here considered. The computational domain (Fig. 7) consists of a rectangular area (width 2 mm, length 50 mm) with a nucleation sites density equal to 2×10^9 m^{-2}. The maximum number of drops in the domain is about 200,000 and the departing radius is maintained constant at $r_{max} = 0.3$ mm. The droplet sliding acceleration is chosen according to the experimental data by Tancon et al. [30,48]: a value equal to 2.6 m s^{-2} is selected considering the experimental data at the highest vapor velocity (13.8 m s^{-1}), for which the measured droplet departing radius was around 0.9 mm [30, 48]. As shown in Fig. 7, three different areas of 2 × 5 mm^2 were identified along the vapor direction (upper, central and lower areas) to determine the drop-size distribution and the heat flux (average and instantaneous). To evaluate the drop-size distribution and the heat flux in the three different regions (upper, central, and lower) of the surface, the simulation was kept running for 0.6 s, with a variation of the time-averaged heat flux less than 5 %. During the simulation time interval, four complete DWC cycles (nucleation, growth by both direct condensation and coalescence, sliding and renucleation) occurred in the considered three areas. The results are reported in Fig. 8.

As shown in Fig. 8a, the drop-size density calculated upon the three selected areas of the surface is affected by the sliding droplets. Close to the equivalent radius r_e (3 μm < r < 9 μm), the number of small droplets in the upper area is slightly lower compared to the central and lower regions. This means that the surface renewal rate is higher in those two areas due to the presence of the sliding drops. For droplet radii larger than 30 μm, the distributions appear to be scattered as compared to the Le Fevre and Rose model [27]. As observed by Tancon et al. [30], this is due to the suddenly variation of the drops dimensions once a sliding droplet enters the investigated area (bin-hopping). In their work, Tancon et al. [30] compared the experimental data with the empirical model by Tanasawa and Ochiai [28] and with the semi-empirical model by Le Fevre and Rose [27]. They found that, when the droplet size exceeds 50 μm, the Le Fevre and Rose [27] model, differently from the model by Tanasawa and Ochiai [28], deviates from the experimental data, because it does not account for the effect of sliding drops on the drop-size distribution. In fact, when the drops in the considered area are removed by the sliding droplets coming from the upper part of the surface, they suddenly disappear from the statistical bin (radii range) in which they were classified, and new drops of smaller size appear. It should be noted that the drop-size distribution proposed by Le Fevre and Rose [27] considers an average behavior of the surface assuming that the droplets disappear once they reach the departure size, without

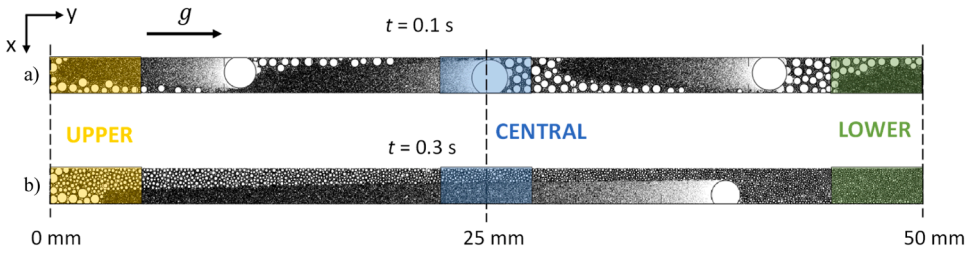

Fig. 7. Simulated droplet population considering a computational domain of 2 × 50 mm^2 at two different time step a) $t = 0.1$ s and b) $t = 0.3$ s with a fixed acceleration equal to 2.6 m s^{-2}. The maximum radius for the simulation is $r_{max} = 0.3$ mm. The three different zones selected on the computation domain (upper, central, and lower) with the same area equal to 2 × 5 mm^2 are highlighted in yellow, blue, and green, respectively. The surface is vertically positioned, as can be seen from the gravity acceleration.

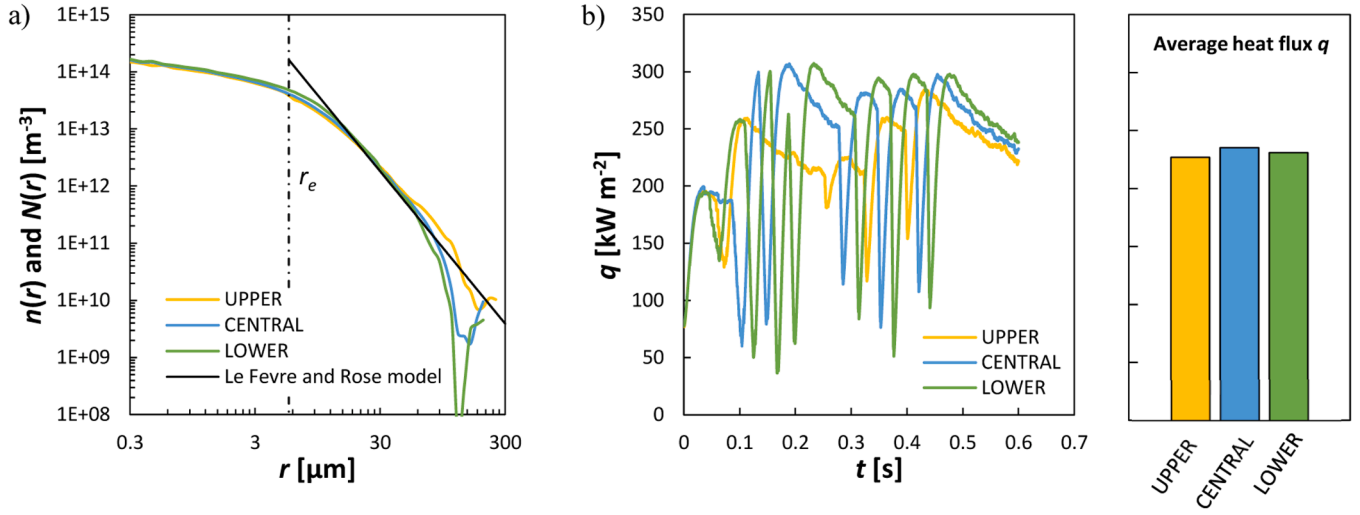

Fig. 8. (a) Drop-size distribution evaluated in the three positions of the computational domain (upper, central and lower). The Le Fevre and Rose equation [27] with $r_{max} = 0.3$ mm is also reported for comparison. (b) Instantaneous and time-averaged heat flux in the three positions of the computational domain. The three colours yellow, blue, and green correspond respectively to the upper, central and lower areas.

considering the sliding effect that influence the droplets below. Coherently, as shown in Fig. 8a, for $r > 30$ µm, the drop-size distribution calculated in the upper area is much closer to theoretical distribution proposed by Le Fevre and Rose [27] as compared to the distributions evaluated in the other two regions. In fact, the drops in the upper area have enough time to reach the departure radius before they start to slide, cleaning the underlying surface. Instead, in the central and lower regions, the drops are usually removed by the sliding drops coming from the upper area before reaching the possible maximum dimension.

The heat flux is also affected by the presence of sliding droplets. Fig. 8b shows that the instantaneous heat flux varies because of the sliding droplets and this variation increases when moving from the upper to the lower area of the surface. In the upper area, the instantaneous heat flux ranges between 120 and 280 kW m^{-2}, while the heat flux evaluated in the lower area varies between 50 and 300 kW m^{-2} due to the presence of sliding drops coming from the upper regions of the surface. Furthermore, it can be observed that the minima of the instantaneous heat flux in the central and lower areas are shifted in time. In fact, as shown in Fig.7b, the sliding drops clean the central area first and then sweep the lower area. Fig. 8c shows the time-averaged heat flux calculated over the entire simulation upon the three considered areas. It is interesting to note that the average heat flux calculated over the entire computational domain is equal to 234 kW m^{-2}, while the local values on the three areas of Fig. 7 are respectively equal to 226, 235 and 230 kW m^{-2} in the upper, central and lower spots. This result highlights that the value of the mean heat flux may be slightly influenced by the position considered within the computational domain. The condensation performance of the central area is the highest and this can be explained considering that: compared to the upper area, the central region is renewed more frequently; in the lower area, the sliding drops have larger sizes, which are associated to higher thermal resistances.

To summarize, both the drop-size distribution and the heat flux display an effect of the sliding drops and thus the position along the computation domain (in particular near r_e and near r_{max} as can be seen in Fig. 8a).

4. Comparison with experimental data

In this Section, the experimental apparatus used to investigate dropwise condensation on vertically oriented metallic specimens is briefly described [30]. Then, the results obtained by the present IBM (both the heat flux and the drop-size distribution) are compared against some data acquired on this experimental apparatus.

4.1. Experimental procedure

The experimental apparatus is the two-phase thermosiphon loop illustrated in Fig. 9a. Briefly, the vapor is generated inside a boiling chamber by means of two electric resistances (maximum electric power equal to 6 kW). Then, it flows through stainless steel pipes (heated by electrical resistances) to the test section, where it partially condenses on a metallic vertically installed specimen (with a surface of 50 × 20 mm^2). Inside the test section, heat transfer measurements and visualizations are performed simultaneously. The surface of the sample exposed to the

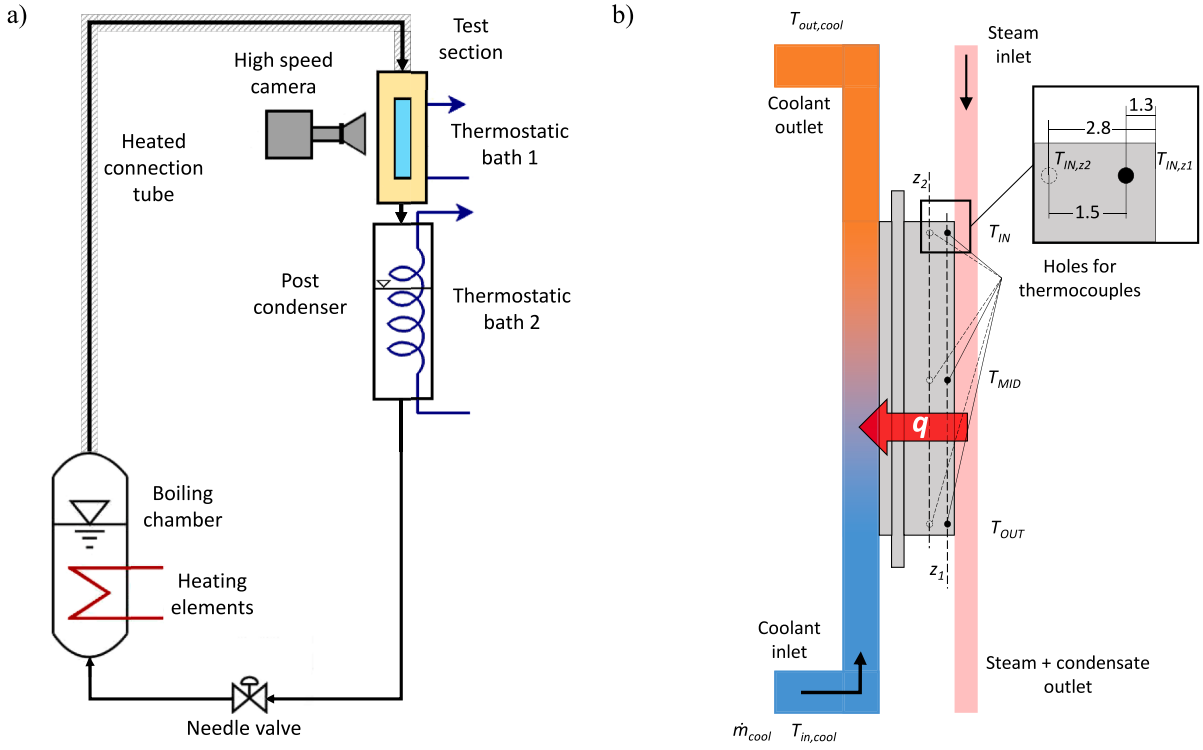

Fig. 9. Experimental apparatus. a) Schematic view of the thermosyphon loop; (b) sketch of the longitudinal cross section of the test section, with the position of the 6 thermocouples inside the metallic sample (dimensions in mm). The directions of the steam and water flows are also depicted.

steam is first mirror polished [7] and subsequently functionalized with a silica-based coating obtained with the sol-gel method [67,68]. In the test section, the condensation heat is released to the water flowing on the back of the sample, which is provided by a thermostatic bath at controlled flow rate and temperature. Downstream of the test section, the two-phase mixture is completely condensed and subcooled inside the post-condenser. Finally, the liquid water returns to the boiling chamber closing the circuit. Steady-state conditions are maintained during the tests. The vapor velocity in the thermosiphon loop is controlled by varying the heating power in the boiling chamber. When the power supplied by the boiling chamber increases from 1 to 5 kW, the vapor velocity in the test section varies in the range 3–15.5 m s^{-1}.

The average heat flux (q) obtained from the energy balance at the coolant side of the test section can be expressed as:

$$q = \frac{\dot{m}_{cool}\, c_p\, \Delta T_{cool}}{A} \tag{27}$$

where ΔT_{cool} is the temperature difference between the inlet and outlet of the coolant, $\dot{m}_{cool}$ is the coolant mass flow rate, c_p is the coolant specific heat capacity, and A is the condensation surface area (50 × 20 mm^2). The average heat flux obtained from the energy balance is compared with the mean heat flux determined by applying the Fourier's law to thermocouples embedded in the substrate at the two different depths z_1 and z_2 as:

$$q = \frac{1}{3}\sum_{i=IN,MID,OUT}\left[\lambda_{AL}\frac{T_{z_1,i} - T_{z_2,i}}{z_2 - z_1}\right] \tag{28}$$

where λ_{AL} is the thermal conductivity of the aluminum substrate, $T_{z1,i}$ is the thermocouple reading at z_1, and $T_{z2,i}$ is the thermocouple reading at z_2. Further details about the procedure are provided in [69]. The deviations between the heat flux value obtained from the two techniques result lower than 6 %.

In order to calculate the HTC, the local surface temperatures ($T_{wall,i}$) at the three different locations (inlet, middle and outlet) are calculated applying the Fourier's law as:

$$T_{wall,i} = T_{z_1,i} + q\frac{z_1}{\lambda_{AL}} \tag{29}$$

where the q is the average heat flux calculated by the energy balance at the coolant side (Eq. (27)).

Thus, the average HTC along the sample length during DWC is evaluated as:

$$\mathrm{HTC} = \frac{q}{\frac{1}{3}\sum\left(T_{sat} - T_{wall,i}\right)} \tag{30}$$

where T_{sat} is the saturation temperature of the vapor. The thermodynamic properties are calculated using the software REFPROP v10 [64]. Each data point reported in this paper was evaluated as the average of 480 readings acquired at 1 Hz. The experimental uncertainties of the main measured parameters were calculated following the procedure reported in the ISO guide [70], with a coverage factor $k = 2$. More details about the uncertainty analysis are provided in [30,48,69].

4.2. Droplet population

To assess the predicted droplet population, the drop-size distribution obtained by the present IBM was compared against the experimental measurements obtained using the visualization technique proposed by Tancon et al. [30] (the operating conditions of the test are listed in Table 1). Natural-size and magnified videos acquired during DWC using a high-speed camera were analysed to map the droplet population with radii from 10 μm to a few millimetres. Each video consists of 2180 frames acquired at 1000 fps. The experimental drop-size distribution was analysed using a program written in MATLAB® that exploits the Image Processing Toolbox plugin. As shown in Daskiran et al. [71] and in Parin et al. [7] each frame is binarized using an optimized brightness threshold value and filtered with the *imerode* and *imdilate* functions to reduce the noise of the black and white image. The annular ring

projected by the annular illumination LED systems over the drops improves the droplets detection capability of the program (more details on the illumination system can be found in Parin et al. [7]). By identifying clusters of pixels, the MATLAB® program is able to identify both the centre and the external radius of each light ring reflected onto the drops. The radius detected by the program is then corrected using an appropriate calibration function that links the external radius of the light ring to the real radius of the droplet. Further details on the procedure can be found in [7,15,72]. Drop-size distribution is achieved by dividing the entire radii range into multiple intervals and counting the number of droplets whose size falls within that specific interval of radii. The frequency histograms determined for each frame are averaged over all the frames analysed and thus detecting the shape of the drop-size distribution. The same methodology was used to determine the distribution starting from the present IBM. More details are reported in Section 3.3. As described in Parin et al. [7], the experimental uncertainty of the drop-size distribution can be determined by Monte Carlo simulations [73]: for the present experimental data the calculated uncertainty is around 12 %.

In Fig. 10, the experimental drop-size distribution measured at $v_v = 13.8$ m s^{-1} using the experimental technique presented by Tancon et al. [30] is compared against the drop-size distribution predicted by the present IBM (Section 3.3). For comparison, the Le Fevre and Rose [27] model (Eq. (24)) is also depicted. The test conditions at which the measurements were performed (Table 1) have also been used as input parameters for the present numerical model. As mentioned in Section 3.2, the use of a long time step does not allow adequate characterization of the small droplet population. However, it has been numerically observed that the discretization of the small droplet distribution is a function of both the time step (as shown in Section 3.2) and the number of nucleation sites. The higher the nucleation sites density, the smaller the time step to be used. Therefore, to predict both the overall heat flux and the drop-size distribution $n(r)$ and $N(r)$, the simulation was performed using a time step $\Delta\tau = 10^{-5}$ s, a computational domain at 1.5 × 1.5 mm^2, a departure radius at $r_{max} = 0.7$ mm and a number of nucleation sites of 5 × 10^{12} m^{-2}. For these boundary conditions, the maximum number of drops within the computational domain is equal to 11 × 10^6. The optimized IBM took approximately 40 days to simulate 1.5 s of DWC (CPU AMD EPYC ™ 7282 16C/32T). This enormous calculation time is necessary to obtain a direct comparison with the experimental data on a surface on which the drops can reach a maximum departing radius of 0.7 mm. The choice of the proper departure radius was made according to the study performed by Tancon et al. [30]. Fig. 10 shows that, even using the state-of-the-art visualization technique and an automatic software for droplet identification, the experimental visualization with pure steam can only detect the large droplet population, detecting drops down to 10 μm radius. To describe the zone of separation between the two distributions (of small and large drops), the optical system should be able to detect droplet sizes that are at least 2 orders of magnitude smaller compared to the current visualization technique. Therefore, only a part of the experimental drop-size distribution of large drops can be compared with the results of the numerical simulations.

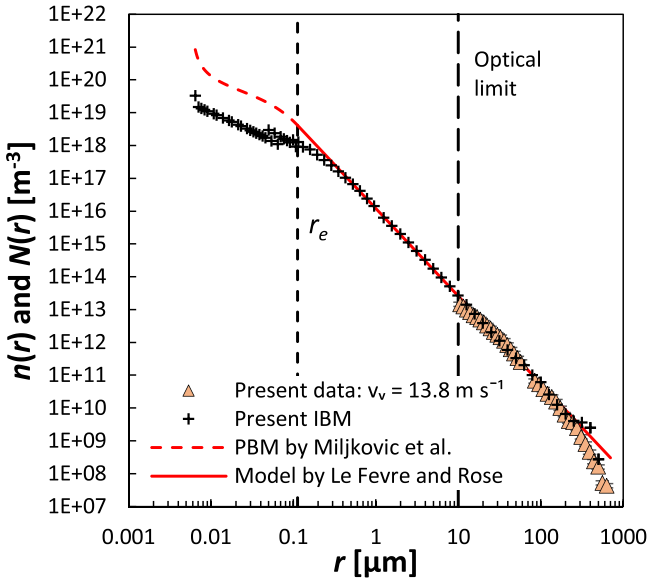

Fig. 10. Comparison between the IBM drop-size distributions (black crosses), the Le Fevre and Rose equation (Eq. (24), red solid line) for the distribution of large droplets, the PBM by Miljkovic et al. [22] equation (Eq. (25), red dashed line) for the distribution of small drops, and the present experimental measurements acquired at $v_v = 13.8$ m s^{-1}. The operating conditions are reported in Table 1. The limit of the current optical system in the present experimental apparatus is depicted. The effective radius calculated by Eq. (23) ($r_e = 0.11$ μm) is also displayed.

As shown in Fig. 10, the two drop-size distributions obtained from both numerically and experimentally procedures are in excellent agreement with the Le Fevre and Rose [27] model in the range of droplet radii from 10 μm to the experimental maximum radius, which, is equal to 0.7 mm at the vapor velocity of 13.8 m s^{-1}. With the use of the present IBM from Fig. 10, three different zones of the drop-size distribution function can be identified. The first corresponds to the smallest droplets in which the main growth mechanism is the direct condensation of the vapor phase (r_{min} to 0.04 μm). The second zone is related to the largest drops growing mainly by coalescence, i.e. for radii ranging from 0.3 μm to r_{max}. Between these two zones (0.04 μm to 0.3 μm), there is an intermediate zone in which the two growth mechanisms interact with each other [38]. This zone is not considered in the traditional statistical models present in the literature, because the resolution of the population balance theory considers a single value of radius (r_e) as the threshold value between the two growth mechanisms.

4.3. Heat transfer

To compare the numerical results with the heat flux measurements performed in the present work, the instantaneous heat flux obtained by the proposed IBM is averaged over the simulation period of 1.5 s. The experimental data refer to dropwise condensation of pure steam at varying vapor velocities (from 3 to 15.5 m s^{-1}), while maintaining the heat flux constant at about 400 kW m^{-2}. In particular, to speed up the calculation times, the present comparison is focused on the heat transfer measurements obtained at a vapor velocity of 13.8 m s^{-1}. When the vapor velocity is equal to 13.8 m s^{-1}, the maximum departing radius observed during DWC (r_{max} = 0.7 mm) is 45 % smaller than that measured at 3 m s^{-1} (r_{max} = 1.24 mm). The smaller the maximum droplet radius, the smaller the minimum size of the domain to be simulated and thus, the faster the calculation time. The literature regarding the number of nucleation sites during pure vapor DWC is scarce. Rose [74] in 1976 proposed a correlation to calculate the number of nucleation sites as a function of the minimum radius $N_s = 0.037 \times r_{min}^{-2}$. However, it is well-known that this expression overestimates the nucleation sites' density [75]. On the other hand, the experimental values of the nucleation site density were found to be in the range from 10^9 m^{-2} to 10^{15} m^{-2} [21,75]. As shown in Fig. 6, the choice of the number of nucleation sites heavily affects the overall heat flux. Using the conditions reported in Table 1, the heat flux calculated by the present IBM varies from 150 to 550 kW m^{-2} in the range of N_s from 10^9 m^{-2} to 10^{15} m^{-2}. Tancon et al. [30] compared their experimental data with the heat flux calculated by the PBM proposed by Miljkovic et al. [22] coupled with the Chavan et al. [23] model for the single droplet heat transfer. The authors observed that using a number of nucleation sites equal to 10^{12} m^{-2} the results of the PBM were comparable with the experimental data. However, as shown in Fig. 6, the use of a PBM leads to higher values of heat flux compared to the IBM due to the

overestimation of the number of drops close to r_e. Therefore, to obtain the same experimental heat flux ($\sim$ 400 kW m^{-2}) the numerical simulation has to use a higher number of nucleation sites with respect to Tancon et al. [30]. It should be noted that the determination of the correct number of nucleation sites is very challenging because it does not depend only on the thermodynamic conditions but also on the characteristics of the coating layer. Hence, the simulation used for comparison with the experimental data adopts the following numerical parameters: time step at $\Delta\tau = 10^{-5}$ s, computational domain at 1.5 $\times$ 1.5 mm^2, departure radius at $r_{max} = 0.7$ mm, and a number of nucleation sites equal to 5 $\times$ 10^{12} m^{-2}. While the other conditions are those reported in Table 1.

Fig. 11 shows a comparison between the experimental and simulated evolution of the droplet population. As already mentioned in Section 3.3, the DWC evolution depends on the droplets growth rate and on the chosen number of nucleation sites. Section 3.3 as the nucleation sites density increases, more coalescences occur among droplets, resulting in a faster droplet growth rate. This comparison is used to determine the reliability of the growth rate calculated from the combination of the Lethuillier et al. [24] model and the chosen N_s value, which should match the experimental observations. It is important to note that this analysis is limited to two specific frames, and thus the comparison in Fig. 11b and Fig. 11d cannot be considered as a validation of the whole model but it provides a comparison between the simulated droplet growth rate and the experimental one. At the initial time ($t = 0$ s), two images have been identified to have the calculated droplet population that adequately matches the experimental droplet population obtained using the high-speed camera (Section 4.2) in terms of droplet dimension. As shown in the first graph of Fig. 11, the drop-size frequency distribution and the maximum drop radius evaluated from the video frame are comparable with those given by the simulation. After 0.1 s, the droplets have grown through the two growth mechanisms: direct condensation and coalescence. As shown in Fig. 11d, the largest drops that can be detected both in the simulation and the experimental visualization are in the radius range from 80 to 100 μm. This demonstrates that, under the same conditions (Table 1), the numerical simulation performed assuming N_s = 5 $\times$ 10^{12} m^{-2} is able to approximate the growth of real droplets during pure steam DWC.

Fig. 12a shows the instantaneous heat flux evaluated by the numerical simulation over 1.5 s of dropwise condensation, in which one sliding event occurs. The evolution of the instantaneous heat flux with time has been linked to the images of the droplet population simulated

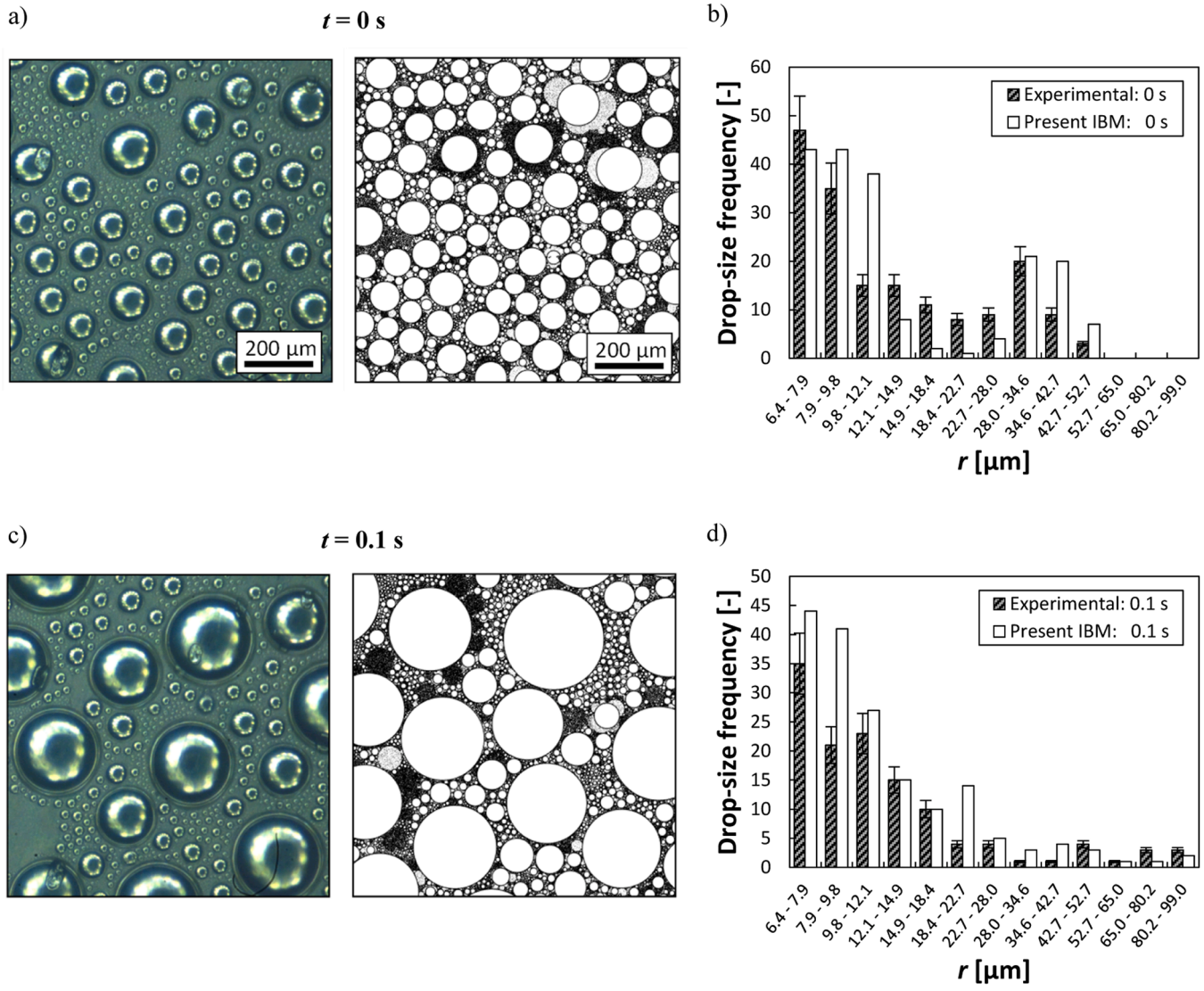

Fig. 11. Droplet population. (a), (c) Population obtained from experimental visualizations (v_v = 13.8 m s^{-1}) and from numerical simulations upon the same area (1.5 $\times$ 1.5 mm^2) at two time steps. (b), d) Drop-size frequency distribution evaluated from images a) and c). The boundary conditions are the ones of Table 1. The simulation was performed with $\Delta\tau = 10^{-5}$ s and $N_s = 5 \times 10^{12}$ m^{-2}.

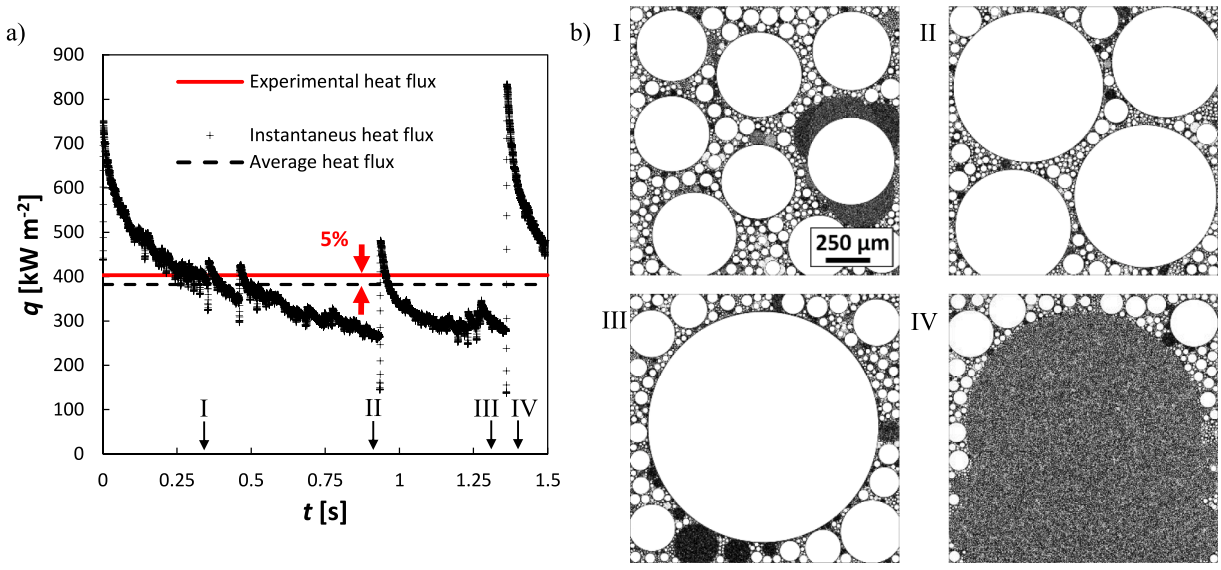

Fig. 12. (a) Instantaneous ($\tilde{q}$) and average (q) heat flux (black dashed line) calculated by the present IBM (Section 3.3) coupled with the single drop heat transfer model by Lethuillier et al. [24] compared against the experimental data (red solid line). The experimental heat flux is equal to 403 kW m^{-2} with an experimental uncertainty of ± 15 kW m^{-2} (b) Time evolution of the droplet population simulated by the present IBM. The test conditions for both the experimental and the IBM are listed in Table 1.

by the present IBM by means of roman numerals (Fig. 12b). When large drops cover the surface (Fig.12b II and III), the heat flux is at the minimum value (about 130 kW m^{-2}) because the thermal resistance due to conduction inside the drops is high; once the surface has been renewed (Fig.12b IV), the conduction resistance through the drop becomes negligible, causing a rapid increase in the heat flux (up to 800 kW m^{-2}). Fig.12a shows that the instantaneous heat flux has an almost cyclic behavior after a sliding event [44,46]. With a computational domain slightly larger than the maximum diameter ($2 \times r_{max}$), the underlying surface is almost completely renewed once the sliding event occurs. Immediately after the droplet sliding, the instantaneous heat flux shows a peak at around 800 kW m^{-2} (at 1.36 s). As shown in Fig.12a, the average heat flux calculated by the simulation is in good agreement with the measurements on an aluminum coated surface ($\theta_{adv} = 87°$ and $\theta_{rec} = 67°$). In particular, the deviation between the numerical and experimental heat flux is equal to 5 %. It must be noted that the average heat flux calculated by the simulation on the area of 1.5×1.5 mm^2 should be associated to the upper area of the condensing surface where there is no influence of the droplets falling, while the experimental heat flux is an average over the total area of the sample (20×50 mm^2) and therefore is affected by the sliding drops. In fact, as shown in Section 3.4, the heat flux in the upper zone may be slightly lower than the average heat flux calculated in the whole area. However, under these operating conditions ($N_s = 5 \times 10^{12}$ m^{-2} and $r_{max} = 0.7$ mm) the magnitude of the heat flux variation due to the position within the computational domain is not known.

Since the present IBM coupled with the model for the heat transfer through single drop by Lethuillier et al. [24] is able to predict the overall heat transfer performance during DWC on a nearly hydrophobic surface ($\theta < 90°$), it could be a valuable tool for obtaining information on the sub-processes involved during the DWC process such as the evolution of the small drops that cannot be experimentally evaluated. By using the Lethuillier et al. [24] model, the present IBM can be employed for contact angles ranging from 20° to 170°, Biot numbers ranging from 10^{-4} to 10^5 and flat surfaces without micro/nanostructure. Furthermore, the assumption of instantaneous coalescence and the re-nucleation phenomena is used. In addition, by matching the predicted heat flux to the experimental value, it can be used to obtain more accurate estimations of the nucleation sites density compared to the PBMs. Although the present IBM coupled with Lethuillier et al.'s single droplet heat transfer model [24] provides results that are in agreement with experimental data, for future developments, it would be possible to couple the present algorithm with a CFD solver and assess the effect of coalescence dynamics on the total heat flux transferred during steam DWC.

5. Conclusions

In this study, a new individual-based model (IBM) to simulate dropwise condensation phenomenon is presented. The model, developed in hybrid MATLAB® and C programming languages with the implementation of the OpenMP library for parallel computing, allows to simulate more than 10 million drops. The main findings are listed below.

- The computation efficiency of the present model was improved by 10–100 times compared to other IBMs for DWC in the literature [41,43,44].
- In order to correctly characterize the drop-size distribution (of both small and large droplets), the time step used in the present IBM must be smaller than 5×10^{-5} s. On the other hand, the overall heat flux can be accurately predicted considering a time step up to 10^{-3} s, thus improving the efficiency of the simulation by 10 times as compared to the case when the time step is 10^{-5} s.
- A comparison was made between the results obtained from three population-based models (PBMs) available in the literature and the present individual-based model (IBM) coupled with the single drop heat transfer model by Lethuillier et al. [24]. The PBMs were found to overestimate the drop-size distribution for radii close to r_e, leading to a 30 % higher heat flux prediction compared to the present IBM, due to the overestimation of the small droplet population.
- The present IBM allows to investigate the effect of sliding drops on the distribution and HTC along a vertically oriented surface, accounting for non-zero droplet acceleration. The computational domain has a height-to-width ratio of 25. The time-averaged heat flux varies along the surface due to sliding droplets coming from the upper part of the domain. The average heat flux calculated over three areas (upper, central, and lower) displayed a variation of about 4 % on such a high aspect ratio surface, with the maximum value in the central region.

- The present IBM coupled with the Lethuillier et al. [24] model for the single droplet heat transfer was compared in terms of droplet population and heat flux against the experimental data acquired using the experimental technique presented by Tancon et al. [30]. The numerical simulation was performed with a nucleation size density of 5×10^{12} m^{-2} (11×10^6 maximum drops in the computational domain) and a time step of 10^{-5} s. For drop radii between 10 μm and r_{max}, the experimental data are in excellent agreement with the simulated drop-size distribution following the power law proposed by Le Fevre and Rose [27]. It is not possible to compare the distribution at lower radius due to the detection difficulties at low drop size. However, the deviation between the mean heat flux calculated by the model and the experimental value is about 5 %.

CRediT authorship contribution statement

Matteo Mirafiori: Methodology, Software, Formal analysis, Investigation, Writing – original draft. **Marco Tancon:** Methodology, Investigation, Formal analysis, Writing – original draft. **Stefano Bortolin:** Conceptualization, Methodology, Writing – review & editing, Supervision. **Davide Del Col:** Conceptualization, Writing – review & editing, Supervision, Funding acquisition.

Declaration of Competing Interest

The authors declare the following financial interests/personal relationships which may be considered as potential competing interests:

Davide Del Col reports financial support was provided by European Space Agency.

Data availability

Data will be made available on request.

Acknowledgments

The authors acknowledge the financial support of the Department of Industrial Engineering of the University of Padova through the BIRD 217032 project (2021). The European Space Agency is greatly acknowledged for supporting this work through the MAP project ENCOM-4 (AO-2004–096).

References

[1] J.M. Beér, High efficiency electric power generation: the environmental role, Prog. Energy Combust. Sci. 33 (2007) 107–134, https://doi.org/10.1016/J.PECS.2006.08.002.

[2] A. Haryanto, S. Fernando, N. Murali, S. Adhikari, Current status of hydrogen production techniques by steam reforming of ethanol: a review, Energy Fuels 19 (2005) 2098–2106, https://doi.org/10.1021/EF0500538/ASSET/IMAGES/LARGE/EF0500538F00003.JPEG.

[3] Y. Ghalavand, M.S. Hatamipour, A. Rahimi, A review on energy consumption of desalination processes, Desalin. Water Treat. 54 (2015) 1526–1541. 10.1080/19443994.2014.892837.

[4] S. Wang, X. Yu, C. Liang, Y. Zhang, Enhanced condensation heat transfer in air-conditioner heat exchanger using superhydrophobic foils, Appl. Therm. Eng. 137 (2018) 758–766, https://doi.org/10.1016/J.APPLTHERMALENG.2018.04.020.

[5] A. Goswami, S.C. Pillai, G. McGranaghan, Surface modifications to enhance dropwise condensation, Surf. Interfaces 25 (2021), 101143, https://doi.org/10.1016/J.SURFIN.2021.101143.

[6] B. El Fil, G. Kini, S. Garimella, A review of dropwise condensation: theory, modeling, experiments, and applications, Int. J. Heat Mass Transf. 160 (2020), 120172, https://doi.org/10.1016/j.ijheatmasstransfer.2020.120172.

[7] R. Parin, M. Tancon, M. Mirafiori, S. Bortolin, L. Moro, L. Zago, F. Carraro, A. Martucci, D. Del Col, Heat transfer and droplet population during dropwise condensation on durable coatings, Appl. Therm. Eng. 179 (2020), 115718, https://doi.org/10.1016/j.applthermaleng.2020.115718.

[8] P.G. De Gennes, F. Brochard-Wyart, D. Quéré, others, Capillarity and Wetting phenomena: drops, bubbles, pearls, Waves, Springer, 2004.

[9] S. Bortolin, M. Tancon, D. Del Col, Heat Transfer Enhancement During Dropwise Condensation Over Wettability-Controlled Surfaces, Springer International Publishing, 2022, pp. 29–67, https://doi.org/10.1007/978-3-030-82992-6_3. Surf. Wettability Eff. Phase Chang.Cham.

[10] E. Colusso, M. Tancon, L. Cazzola, R. Parin, S. Agnoli, F. De Boni, M.G. Pelizzo, E. Della Gaspera, D. Del Col, A. Martucci, Solution-processed graphene oxide coatings for enhanced heat transfer during dropwise condensation of steam, Nano Sel. 2 (2021) 61–71, https://doi.org/10.1002/NANO.202000105.

[11] M. Mirafiori, M. Tancon, S. Bortolin, A. Martucci, D. Del Col, Mechanisms of dropwise condensation on aluminum coated surfaces, J. Phys. Conf. Ser. 2177 (2022), 012046, https://doi.org/10.1088/1742-6596/2177/1/012046.

[12] D. Maggiolo, S. Sasic, H. Ström, Self-cleaning compact heat exchangers: the role of two-phase flow patterns in design and optimization, Int. J. Multiph. Flow. 112 (2019) 1–12, https://doi.org/10.1016/J.IJMULTIPHASEFLOW.2018.12.006.

[13] Z. Xu, L. Zhang, K. Wilke, E.N. Wang, Multiscale dynamic growth and energy transport of droplets during condensation, Langmuir 34 (2018) 9085–9095, https://doi.org/10.1021/ACS.LANGMUIR.8B01450.

[14] T.Q. Liu, W. Sun, X.Y. Sun, H.R. Ai, Mechanism study of condensed drops jumping on super-hydrophobic surfaces, Colloids Surf. A Physicochem. Eng. Asp. Complete (2012) 366–374, https://doi.org/10.1016/J.COLSURFA.2012.08.063.

[15] M. Tancon, M. Mirafiori, S. Bortolin, R. Parin, E. Colusso, A. Martucci, D. Del Col, Simultaneous measurement of heat flux and droplet population during dropwise condensation from humid air flowing on a vertical surface, Exp. Therm. Fluid Sci. 136 (2022), 110677, https://doi.org/10.1016/J.EXPTHERMFLUSCI.2022.110677.

[16] L. Zhang, R. Iwata, L. Zhao, S. Gong, Z. Lu, Z. Xu, Y. Zhong, J. Zhu, S. Cruz, K. L. Wilke, P. Cheng, E.N. Wang, Nucleation site distribution probed by phase-enhanced environmental scanning electron microscopy, Cell Rep. Phys. Sci. 1 (2020), 100262, https://doi.org/10.1016/j.xcrp.2020.100262.

[17] A. Katselas, R. Parin, C. Neto, A. Katselas, R. Parin, C. Neto, Quantification of nucleation site density as a function of surface wettability on smooth surfaces, Adv. Mater. Interfaces 9 (2022), 2200246, https://doi.org/10.1002/ADMI.202200246.

[18] J.W. Rose, Dropwise condensation theory, Int. J. Heat Mass Transf. 24 (1981) 191–194, https://doi.org/10.1016/0017-9310(81)90026-0.

[19] J.W. Rose, Dropwise condensation theory and experiment: a review, Proc. Inst. Mech. Eng. A J. Power Energy. 216 (2002) 115–128, https://doi.org/10.1243/09576500260049034.

[20] M. Abu-Orabi, Modeling of heat transfer in dropwise condensation, Int. J. Heat Mass Transf. 41 (1998) 81–87, https://doi.org/10.1016/S0017-9310(97)00094-X.

[21] S. Kim, K.J. Kim, Dropwise condensation modeling suitable for superhydrophobic surfaces, J. Heat Transf. 133 (2011), 081502, https://doi.org/10.1115/1.4003742.

[22] N. Miljkovic, R. Enright, E.N. Wang, Modeling and optimization of superhydrophobic condensation, J. Heat Transf. 135 (2013), 111004, https://doi.org/10.1115/1.4024597.

[23] S. Chavan, H. Cha, D. Orejon, K. Nawaz, N. Singla, Y.F. Yeung, D. Park, D.H. Kang, Y. Chang, Y. Takata, N. Miljkovic, Heat transfer through a condensate droplet on hydrophobic and nanostructured superhydrophobic surfaces, Langmuir 32 (2016) 7774–7787, https://doi.org/10.1021/acs.langmuir.6b01903.

[24] J. Lethuillier, M. Miscevic, P. Lavieille, S. Blanco, C. Coustet, F. Topin, Comprehensive correlation for the prediction of the heat transfer through a single droplet in dropwise condensation regime, Appl. Therm. Eng. 209 (2022), 118233, https://doi.org/10.1016/J.APPLTHERMALENG.2022.118233.

[25] H. Tanaka, A theoretical study of dropwise condensation, J. Heat Transf. 97 (1975) 72–78, https://doi.org/10.1115/1.3450291.

[26] H. Tanaka, Further Developments of Dropwise Condensation Theory, J. Heat Transf. 101 (1979) 603–611, https://doi.org/10.1115/1.3451044.

[27] E.J. Le Fevre, J.W. Rose, A theory of heat transfer by dropwise condensation, in: Proceeding of the International Heat Transfer Conference 3, Begellhouse, Connecticut, 1966, pp. 362–375, https://doi.org/10.1615/IHTC3.180.

[28] I. Tanasawa, J. Ochiai, Experimental study on dropwise condensation, Bull. JSME 16 (1973) 1184–1197.

[29] J.W. Rose, L.R. Glicksman, Dropwise condensation-The distribution of drop sizes, Int. J. Heat Mass Transf. 16 (1973) 411–425, https://doi.org/10.1016/0017-9310(73)90068-9.

[30] M. Tancon, M. Mirafiori, S. Bortolin, M. Basso, E. Colusso, D. Del Col, Dropwise condensation mechanisms when varying vapor velocity, Appl. Therm. Eng. 216 (2022), 119021, https://doi.org/10.1016/J.APPLTHERMALENG.2022.119021.

[31] W.H. Wu, J.R. Maa, A mechanism for dropwise condensation and nucleation, Chem. Eng. J. 11 (1976) 143–146, https://doi.org/10.1016/S0300-9467(76)80036-6.

[32] J.R. Maa, Drop size distribution and heat flux of dropwise condensation, Chem. Eng. J. 16 (1978) 171–176, https://doi.org/10.1016/0300-9467(78)85052-7.

[33] E.J. Le Fevre, J.W. Rose, Bicentenary of the James Watt Patent for a Separate Condenser for the Steam Engine: Proceedings of a Two-Day Symposium, 1-2 September 1969.

[34] D.W. Tanner, D. Pope, C.J. Potter, D. West, Heat transfer in dropwise condensation at low steam pressures in the absence and presence of non-condensable gas, Int. J. Heat Mass Transf. 11 (1968) 181–190, https://doi.org/10.1016/0017-9310(68)90148-8.

[35] L.R. Glicksman, A.W. Hunt, Numerical simulation of dropwise condensation, Int. J. Heat Mass Transf. 15 (1972) 2251–2269, https://doi.org/10.1016/0017-9310(72)90046-4.

[36] S. Boroomandi Barati, N. Pionnier, J.C. Pinoli, S. Valette, Y. Gavet, Investigation spatial distribution of droplets and the percentage of surface coverage during dropwise condensation, Int. J. Therm. Sci. 124 (2018) 356–365, https://doi.org/10.1016/j.ijthermalsci.2017.10.020.

[37] W. Xu, Z. Lan, Q. Liu, B. Du, X. Ma, Droplet size distributions in dropwise condensation heat transfer: consideration of droplet overlapping and multiple re-

nucleation, Int. J. Heat Mass Transf. 127 (2018) 44–54, https://doi.org/10.1016/j.ijheatmasstransfer.2018.07.020.
[38] J. Lethuillier, P. Lavieille, M. Miscevic, About the role of falling droplets' sweeping in surface renewal during dropwise condensation, Langmuir 36 (2020) 12877–12886, https://doi.org/10.1021/acs.langmuir.0c02092.
[39] K.A. Stevens, J. Crockett, D. Maynes, B.D. Iverson, Simulation of drop-size distribution during dropwise and jumping drop condensation on a vertical surface: implications for heat transfer modeling, Langmuir 35 (2019) 12858–12875, https://doi.org/10.1021/acs.langmuir.9b02232.
[40] B.M. Burnside, H.A. Hadi, Digital computer simulation of dropwise condensation from equilibrium droplet to detectable size, Int. J. Heat Mass Transf. 42 (1999) 3137–3146, https://doi.org/10.1016/S0017-9310(98)00372-X.
[41] K. Meng, W. Fan, H. Wang, Dynamic scenario simulation of dropwise condensation on a superhydrophobic surface with droplet jumping, Appl. Therm. Eng. 148 (2019) 316–323, https://doi.org/10.1016/J.APPLTHERMALENG.2018.11.049.
[42] R. Wen, Q. Li, J. Wu, G. Wu, W. Wang, Y. Chen, X. Ma, D. Zhao, R. Yang, Hydrophobic copper nanowires for enhancing condensation heat transfer, Nano Energy 33 (2017) 177–183, https://doi.org/10.1016/J.NANOEN.2017.01.018.
[43] M. Mei, F. Hu, C. Han, Y. Sun, D. Liu, Time evolution of the droplet size distribution in dropwise condensation, J. Heat Transf. 142 (2020) 1–12, https://doi.org/10.1115/1.4047488.
[44] Z. Hu, Z. Yuan, H. Hou, F. Chu, X.M. Wu, Event-driven simulation of multi-scale dropwise condensation, Int. J. Heat Mass Transf. 167 (2021), 120819, https://doi.org/10.1016/j.ijheatmasstransfer.2020.120819.
[45] H. Cha, H. Vahabi, A. Wu, S. Chavan, M.K. Kim, S. Sett, S.A. Bosch, W. Wang, A. K. Kota, N. Miljkovic, Dropwise condensation on solid hydrophilic surfaces, Sci. Adv. 6 (2020), https://doi.org/10.1126/sciadv.aax0746 eaax0746.
[46] B. Singh Sikarwar, S. Khandekar, K. Muralidhar, Mathematical modelling of dropwise condensation on textured surfaces, Sadhana - Acad. Proc. Eng. Sci. 38 (2013) 1135–1171, https://doi.org/10.1007/s12046-013-0190-9.
[47] S. Anand, S.Y. Son, Sub-micrometer dropwise condensation under superheated and rarefied vapor condition, Langmuir 26 (2010) 17100–17110, https://doi.org/10.1021/LA102642R.
[48] M. Tancon, R. Parin, S. Bortolin, A. Martucci, D. Del Col, Effect of steam velocity during dropwise condensation, Int. J. Heat Mass Transf. 165 (2021), 120624, https://doi.org/10.1016/j.ijheatmasstransfer.2020.120624.
[49] G. Chkonia, J. Wölk, R. Strey, J. Wedekind, D. Reguera, Evaluating nucleation rates in direct simulations, J. Chem. Phys. 130 (2009), 064505, https://doi.org/10.1063/1.3072794.
[50] E.E. Gose, A.N. Mucciardi, E. Baer, Model for dropwise condensation on randomly distributed sites, Int. J. Heat Mass Transf. 10 (1967) 15–22, https://doi.org/10.1016/0017-9310(67)90180-9.
[51] K. Yasuoka, M. Matsumoto, Molecular dynamics of homogeneous nucleation in the vapor phase. II. Water, J. Chem. Phys. 109 (1998) 8463–8470, https://doi.org/10.1063/1.477510.
[52] D.T.S. Ranathunga, A. Shamir, X. Dai, S.O. Nielsen, Molecular dynamics simulations of water condensation on surfaces with tunable wettability, Langmuir. 36 (2020) 7383–7391. 10.1021/ACS.LANGMUIR.0C00915/ASSET/IMAGES/LARGE/LA0C00915_0006.JPEG.
[53] E. Bird, J. Gutierrez Plascencia, P. Keblinski, Z. Liang, Molecular simulation of steady-state evaporation and condensation of water in air, Int. J. Heat Mass Transf. 184 (2022), 122285, https://doi.org/10.1016/J.IJHEATMASSTRANSFER.2021.122285.
[54] V.P. Carey, Liquid-Vapor Phase-Change Phenomena: An Introduction to the Thermophysics of Vaporization and Condensation Processes in Heat Transfer Equipment, 3rd Ed., CRC Press, 2020.
[55] A.F. Mills, R.A. Seban, The condensation coefficient of water, Int. J. Heat Mass Transf. 10 (1967) 1815–1827, https://doi.org/10.1016/0017-9310(67)90052-X.
[56] B. Paul, Compilation of evaporation coefficients, ARS J. 32 (1962) 1321–1328, https://doi.org/10.2514/8.6277.
[57] H. Kim, J. Buongiorno, Detection of liquid–vapor–solid triple contact line in two-phase heat transfer phenomena using high-speed infrared thermometry, Int. J. Multiph. Flow 37 (2011) 166–172, https://doi.org/10.1016/J.IJMULTIPHASEFLOW.2010.09.010.
[58] D. Niu, L. Guo, H.W. Hu, G.H. Tang, Dropwise condensation heat transfer model considering the liquid-solid interfacial thermal resistance, Int. J. Heat Mass Transf. 112 (2017) 333–342, https://doi.org/10.1016/J.IJHEATMASSTRANSFER.2017.04.061.
[59] S. Adhikari, A.S. Rattner, Heat transfer during condensing droplet coalescence, Int. J. Heat Mass Transf. 127 (2018) 1159–1169, https://doi.org/10.1016/j.ijheatmasstransfer.2018.07.005.
[60] M. Irshad Khodabocus, M. Sellier, V. Nock, Scaling laws of droplet coalescence: theory and numerical simulation, Adv. Math. Phys. 2018 (2018), https://doi.org/10.1155/2018/4906016.
[61] M. Tancon, M. Mirafiori, S. Bortolin, A. Martucci, D. Del Col, Droplet sweeping to enhance heat transfer during dropwise condensation, J. Phys. Conf. Ser. 2116 (2021), 012013, https://doi.org/10.1088/1742-6596/2116/1/012013.
[62] J. Xie, J. Xu, W. Shang, K. Zhang, Mode selection between sliding and rolling for droplet on inclined surface: effect of surface wettability, Int. J. Heat Mass Transf. 122 (2018) 45–58, https://doi.org/10.1016/j.ijheatmasstransfer.2018.01.098.
[63] G.K. Batchelor, An Introduction to Fluid Dynamics, Cambridge University Press, 2000, https://doi.org/10.1017/CBO9780511800955.
[64] E.W. Lemmon, I.H. Bell, M.L. Huber, M.O. McLinden, NIST Standard reference database 23: reference fluid thermodynamic and transport properties-REFPROP 10. https://doi.org/10.18434/T4/1502528.
[65] P.M. Dixon, Ripley's K Function, Wiley StatsRef: Statistics Reference Online, John Wiley & Sons, Ltd, Chichester, UK, 2014, https://doi.org/10.1002/9781118445112.stat07751.
[66] T. Andrews, Computation Time Comparison Between Matlab and C++ Using Launch Windows, Aerosp. Eng. (2012) 1–6. https://digitalcommons.calpoly.edu/aerosp/78 (accessed December 28, 2023).
[67] M. Basso, E. Colusso, M. Tancon, S. Bortolin, M. Mirafiori, M. Guglielmi, D. Del Col, A. Martucci, Hydrophobic hybrid silica sol-gel coating on aluminium: stability evaluation during saturated vapour condensation, J. Non Cryst. Solids X 17 (2023), https://doi.org/10.1016/J.NOCX.2022.100143.
[68] M. Basso, E. Colusso, A. Sacco, M. Tancon, S. Bortolin, M. Mirafiori, M. Guglielmi, A. Martucci, Bioinspired silica-based sol–gel micropatterns on aluminium for humid air condensation, J. Sol Gel Sci. Technol. 102 (2022) 466–477, https://doi.org/10.1007/S10971-022-05771-7/FIGURES/6.
[69] A. Bisetto, S. Bortolin, D. Del Col, Experimental analysis of steam condensation over conventional and superhydrophilic vertical surfaces, Exp. Therm. Fluid Sci. 68 (2015) 216–227, https://doi.org/10.1016/J.EXPTHERMFLUSCI.2015.04.019.
[70] Joint Committee for. Guides in Metrology, Evaluation of Measurement Data - Guide to the Expression of Uncertainty in Measurement, Sèvres, France, 2008.
[71] C. Daskiran, R. Liu, K. Lee, J. Katz, M.C. Boufadel, Estimation of overall droplet size distribution from a local droplet size distribution for a jet in crossflow: experiment and multiphase large eddy simulations, Int. J. Multiph. Flow 156 (2022), 104205, https://doi.org/10.1016/J.IJMULTIPHASEFLOW.2022.104205.
[72] M. Mirafiori, R. Parin, S. Bortolin, D. Del Col, Experimental analysis of drop-size density distribution during dropwise condensation of steam, J. Phys. Conf. Ser. 1599 (2020), 012011, https://doi.org/10.1088/1742-6596/1599/1/012011.
[73] P.R. Guimaraes Couto, J. Carreteiro, S.P. de Oliveir, Monte Carlo Simulations Applied to Uncertainty in Measurement, Theory Appl. Monte Carlo Simulations. (2013). 10.5772/53014.
[74] J.W. Rose, Further aspects of dropwise condensation theory, Int. J. Heat Mass Transf. 19 (1976) 1363–1370, https://doi.org/10.1016/0017-9310(76)90064-8.
[75] X. Liu, P. Cheng, Dropwise condensation theory revisited Part II. Droplet nucleation density and condensation heat flux, Int. J. Heat Mass Transf. 83 (2015) 842–849, https://doi.org/10.1016/J.IJHEATMASSTRANSFER.2014.11.008.